



Hull-form stochastic optimization via computational-cost reduction methods

Andrea Serani¹ · Frederick Stern² · Emilio F. Campana³ · Matteo Diez¹

Received: 18 September 2020 / Accepted: 25 February 2021 / Published online: 24 March 2021
© The Author(s), under exclusive licence to Springer-Verlag London Ltd., part of Springer Nature 2021

Abstract

The paper shows how cost-reduction methods can be synergistically combined to enable high-fidelity hull-form optimization under stochastic conditions. Specifically, a multi-objective hull-form optimization is presented, where (a) physics-informed design-space dimensionality reduction, (b) adaptive metamodeling, (c) uncertainty quantification (UQ) methods, and (d) global multi-objective algorithm are efficiently and effectively combined to achieve high-fidelity simulation-based design optimization (SBDO) solutions. The application pertains to the multi-objective optimization for resistance and seakeeping (operational efficiency and effectiveness) of a destroyer-type vessel. Two hierarchical multi-objective SBDO problems are presented, with a level of complexity decreasing from the most general (stochastic sea state, heading, and speed) to the least general (deterministic regular wave, at fixed sea state, heading, and speed). Design-space dimensionality reduction is based on a generalized Karhunen-Loève expansion of the shape modification vector combined with low-fidelity-based physical variables. A multi-objective deterministic particle swarm optimization algorithm is applied to a stochastic radial-basis-function metamodel that provides objective predictions. UQ methods include Gaussian quadrature and metamodel-based importance sampling. Numerical simulations are based on unsteady Reynolds-averaged Navier–Stokes and potential flow solvers. The paper shows and discusses the joint effort of computational-cost reduction methods in enabling high-fidelity SBDO, providing guidelines for future research directions in this area.

Keywords Simulation-based design optimization · Stochastic optimization · Reliability-based robust design optimization · Physics-informed design-space dimensionality reduction · Adaptive metamodeling · Uncertainty quantification · Global multi-objective optimization · Computational fluid dynamics

1 Introduction

Industries along with small- and medium-sized enterprises (SMEs) are facing a fierce competition in envisioning new and highly innovative technologies and products. Their achievement, along with a reduction of design and production costs, represents an enabling factor to win the worldwide-market challenges. In the race for innovative

engineering products, computer simulations are playing an increasingly important role in the design process. Computer simulations need to address real-world problems, often requiring high-fidelity physics-based computational tools along with uncertainty quantification (UQ) methods able to address the unavoidable stochasticity of real-world applications. In this context, the simulation-based design (SBD) paradigm has demonstrated the capability of supporting the design decision process, not only providing large sets of design options but also exploring operational spaces by assessing design performance for large sets of operating and environmental conditions. The continuous development of high-performance computing systems has contributed moving the SBD paradigm toward automatic SBD optimization (SBDO) [15] and simulation-driven (SDD) [22] formulations, where the design process is driven by optimization algorithms, possibly addressing conflicting design objectives and aiming at global solutions to the design problem. SBDO

✉ Andrea Serani
andrea.serani@cnr.it

¹ CNR-INM, National Research Council-Institute of Marine Engineering, Rome, Italy

² IIHR-Hydroscience and Engineering, The University of Iowa, Iowa City, USA

³ CNR-DIITET, National Research Council-Engineering, ICT and Technologies for Energy and Transportation Department, Rome, Italy

has shown a great potential in the development of products whose performance is highly affected by shape parameters (e.g., aerial, waterborne, and ground vehicles, propellers, turbomachineries, channels, ducts, heat exchangers, mechanical parts, building facades, etc.). In shape-design problems, SBDO consists of three main elements (see Fig. 1): (1) an analysis/simulation tool, (2) an optimization algorithm, and (3) a design/shape modification tool.

Despite the unquestionably significant achievements in this area, the computational cost associated with the solution of an SBDO relying on high-fidelity solvers still remains a limiting factor for a widespread use of high-fidelity SBDO in industries and SMEs especially. The main issues concurring to the computational cost of high-fidelity SBDO may be summarized as follows: (a) running high-fidelity physics-based solvers is usually computationally expensive; (b) addressing the problem stochasticity needs UQ methods, which require multiple simulations spanning stochastic operating and environmental conditions; (c) finally, the identification of optimal designs through the optimization process may require evaluating the performance for a large number of designs, especially for high-dimensional design spaces and global multi-objective problems. Recent methods, such as design-space dimensionality reduction techniques, adaptive metamodels, efficient UQ and global optimization methods, have been surfacing to alleviate the computational cost of SBDO providing the foundation for the affordability of high-fidelity SBDO.

The identification of global design optima is certainly a challenging task, especially when one deals with computationally expensive, high-dimensionality, and global multi-objective design problems. In industrial applications, design objectives and constraints are often provided by black-box simulation tools, which usually do not provide function derivatives. Additionally, iterative processes within simulation tools and solution residuals may affect the function smoothness with the unavoidable addition of noise. For this reason derivative-free optimization algorithms [29], such as evolutionary algorithms (EAs) [9] and metaheuristic approaches [66], are often the preferred option. In this context, several derivative-free methods have been proposed to

solve multi-objective problems, such as for instance non-dominated sorting-III [11], dragonfly [37], salp swarm [38], and multi-objective particle swarm optimization (PSO) [7] algorithms. Most methods ensure global exploration and solution diversity by the use of random components. These require running the optimization multiple times, if one wants to achieve statistically significant results. This may not be affordable if computationally expensive simulations are used within SBDO. For this reason, recent research has focused on deterministic metaheuristic approaches, such as the multi-objective deterministic particle swarm optimization (MODPSO) method [41] and its memetic variants [42].

An additional and great challenge associated with solving real-world design optimization problems stems from the unavoidable uncertainty associated with operating and environmental conditions [48]. Design objectives and constraints are rarely (if not never) deterministic and their stochasticity must be taken into account in the SBDO process [61]. A case in point is given by ships and their subsystems, which are required to operate under a variety of operating/sea conditions, such as speed, payload, sea state, and wave heading, all highly stochastic [15]. As a consequence, design objectives and constraints, such as resistance, seakeeping, and maneuverability performance are highly affected by this stochasticity and the design optimization problem must carefully consider their statistics. The accurate quantification of statistical indicators usually requires many function evaluations and therefore efficient UQ methods are essential to the affordability and success of SBDO. The development and application of UQ methods for vehicle problems (including ships) were the subject of the NATO Science and Technology Organization, Applied Vehicle Technology group AVT-191 “Application of Sensitivity Analysis and Uncertainty Quantification to Military Vehicle Design” [57], where the computational UQ of a high-speed catamaran was performed for calm water [16], regular [23], and irregular [13] waves. An experimental UQ was presented in [18] for validation purposes of the same model in regular and irregular waves. The efficiency of UQ methods is generally problem dependent and should be carefully assessed. For this reason, the efficient integration of UQ methods within stochastic design optimization procedures for air and sea vehicles was addressed in the NATO AVT-252 group on “Stochastic Design Optimization for Naval and Aero Military Vehicles” [54], where several UQ methods (including quadrature formulas and metamodel-based methods) were compared on an airfoil benchmark problem [46].

Metamodels (or surrogate models) have been developed with the aim of reducing the computational cost of the optimization process and have been successfully applied in several engineering fields [62], including aerodynamics [25] and ship hydrodynamics [31]. A metamodel emulates the expensive response of some black-box function by

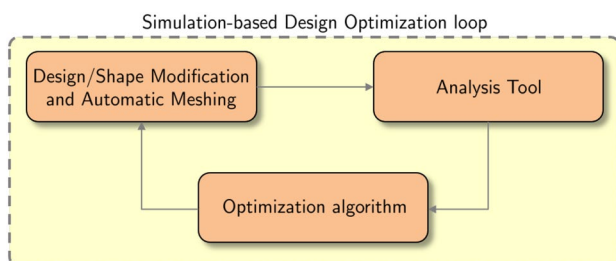


Fig. 1 Basic SBDO scheme

constructing a computationally inexpensive (to evaluate) surrogate. In metamodel-based optimization, two alternative approaches are usually followed, namely static or adaptive/sequential metamodeling [26]. The static approach to metamodeling is the most simple. An a priori design of experiments (DoE) provides the training set used to generate an approximate model of the original objectives and constraints. Efforts are then made to find the optimum/optima of the (static) metamodel, assuming that the optimal solutions of both the metamodel and the original problem are similar to each other [20]. In the adaptive/sequential approach, the search for optimal solutions is iterated over sequential metamodels [12], where new solutions are added to the training set as the optimization progresses. The purpose of performing an adaptive DoE is to add training points where it is most useful, making the training process as efficient as possible. Examples of adaptive metamodels based on Kriging and stochastic radial basis function (SRBF) can be found in [69] and [63], respectively. In global optimization problems, the most effective approach to balance exploration (ensuring global model accuracy) and exploitation (ensuring good optimization convergence) capabilities is problem dependent and remains an open issue [26, 56].

High-dimensional SBDO problems may be reduced in dimensionality using on-line and off-line design-space dimensionality reduction (DR) methods. On-line methods require the evaluation of the objective function or its gradient and are mostly based on principal component analysis (PCA) or proper orthogonal decomposition (POD) [47]. A PCA/POD-type approach is used in the active subspace method [33, 59] to discover and exploit low dimensional monotonic trends in the objective function, based on the evaluation of its gradient. Generally, these methods do not provide the assessment of the design space and associated shape parametrization before optimization is performed or objective function and/or gradient are evaluated. Furthermore they may be not convenient if gradients are not directly provided (i.e., in the case of black-box simulation tools), and their extension to global optimization is not straightforward. Off-line or upfront methods have been developed focusing on the assessment of design-space variability and the subsequent DR before the optimization is performed. A method based on the Karhunen-Loève expansion (KLE, equivalent to POD) has been formulated in [14] for the assessment of the shape modification variability and the definition of a reduced-dimensionality global model of the shape modification vector in hull form optimization. No objective function evaluation nor gradient is required by the method. The KLE is applied to the continuous shape modification vector, requiring the solution of a Fredholm integral equation of the second kind. Once the equation is discretized, the problem reduces to the PCA of discrete geometrical data. Off-line methods improve the shape optimization efficiency by

reparametrization and DR, providing the assessment of the design space and the shape parametrization before optimization and/or performance analysis are carried out. The assessment is based on the geometric variability associated to the design space, making the method computationally very efficient and attractive (no simulations are required). Nevertheless, significant physical phenomena induced by small shape modifications (such as flow separations, regime transitions, etc.) may be overlooked as no physical information is processed by the method. An extension of the off-line method to a physics-informed formulation was introduced in [17]. This extension improves the effectiveness of the DR, bringing physics-based information into the variability breakdown analysis. In order to balance the DR effectiveness with the computational cost of the overall operation, physics-based information is provided by low-fidelity computations [51].

Despite the unquestionable recent developments of computational-cost reduction methodologies, examples of hull-form optimization via high-fidelity simulations (such as Reynolds-averaged Navier–Stokes computations, RANS) are still limited and focus mostly on deterministic single objective problem in calm water. For instance, Campana et al. [4] discussed two approaches to single-objective SBDO of the DTMB 5415 model in calm water, including Bezier surfaces and a CAD-based methods for the shape modification, coupled with genetic algorithm and approximation-model management. Chen et al. [5] presented the total resistance minimization of the Delft catamaran (DC) in calm water by morphing of KLE eigenvectors (coming from a geometry-based dimensionality reduction procedure), deterministic PSO, and several metamodels (namely SRBF, ordinary Kriging, least-square support vector machine, and polyharmonic spline). Tezdogan et al. [58] presented the total resistance optimization of a fishing boat via arbitrary shape deformation (ASD) and a hybrid non linear programming via a quadratic Lagrangian (NLPQL) algorithm. Zhang et al. [68] discussed the total resistance optimization of the DTMB 5415 and Wigley III models via ASD, an improved PSO, and Elman neural networks. Coppedè et al. [8] presented the single-objective optimization of the KRISO containership for total-resistance reduction via a morphing technique based on the free-form deformation (FFD) method, a genetic algorithm, and a Gaussian process response surface. Examples of multi-objective optimization are provided for instance by Yang and Huang [65], who presented of the total resistance optimization of the Series 60 (S60) hull at two speeds, using a multi-objective artificial bee colony algorithm with RBF approaches to both shape modification and metamodeling. Miao et al. [35] proposed a multi-objective total resistance optimization at two speeds for a S60 catamaran via FFD, NSGA-II, and Kriging. An example of optimization in waves can be found in [67],

where the DTMB 5415 and the Wigley III models were optimized for resistance reduction in regular head waves, via ASD and hybrid NLPQL. Finally, an example of multi-objective optimization for resistance and operability subject to stochastic operations and environment, but limited to head waves, was presented in [15], where the DC is optimized via morphing of (geometry-based) KLE eigenvectors, MODPSO, and SRBF.

The objective of the present work is to show and discuss how a synergetic use of computational-cost reduction methods can enable for the solution of complex multi-objective SBDO problems, based on high-fidelity simulations. Specifically, (a) physics-informed design-space DR, (b) adaptive metamodel, (c) UQ methods, and (d) global multi-objective optimization algorithm, are combined for the solution of a hull-form optimization problem subject to stochastic operating and environmental conditions, extending earlier work [15] to variable heading and a more realistic scenario.

The application pertains to the multi-objective optimization of a destroyer-type vessel for resistance reduction and operational effectiveness (operability) improvement. Stochastic sea state and operations in the North Atlantic Ocean scenario are addressed. The parent hull is a naval destroyer design, namely the DTMB 5415 model, extensively used as an international benchmark for computational and experimental fluid-dynamic studies [30], as well as for shape optimization problems [21]. Two hierarchical multi-objective SBDO problems are presented, with a level of complexity decreasing from the most general (stochastic sea state, heading, and speed) to the least general (deterministic regular wave, at fixed sea state, heading, and speed). The design space is defined by three design variables, provided by the physics-informed DR method [51], based on the generalized KLE of geometric modification, pressure distribution, wave elevation, and wave resistance coefficient. Physics information is provided by (low-fidelity and computationally inexpensive) potential flow solvers. The optimization procedure is driven by MODPSO [41] on a SRBF [63] metamodel trained by unsteady RANS and linearized strip theory potential flow solvers, for resistance and seakeeping response, respectively. Finally, UQ methods are applied, and include Gaussian quadrature and metamodel-based importance sampling.

The paper is organized as follows. The general deterministic and stochastic design optimization problems are formulated in Sect. 2, while the computational-cost reduction methods are presented in Sect. 3. Details on the current hull-form optimization problem, simulations, and SBDO settings are provided in Sect. 4. Numerical results and discussion are shown Sects. 5 and 6. Finally, concluding remarks and future work are addressed in Sect. 7.

2 Stochastic design optimization problem

Consider a deterministic design optimization (DDO) problem as

$$\begin{aligned} &\text{minimize } f_k(\mathbf{x}, \mathbf{y}) \\ &\text{subject to } g_n(\mathbf{x}, \mathbf{y}) \leq 0 \\ &\quad \text{and to } h_i(\mathbf{x}) \leq 0 \\ &\quad \text{and to } q_j(\mathbf{x}) = 0 \\ &\quad \text{and to } \mathbf{x}^l \leq \mathbf{x} \leq \mathbf{x}^u, \end{aligned} \tag{1}$$

where $\mathbf{x} \in \mathbb{R}^N$ is the design variables vector (with N number of design variables) bound by \mathbf{x}^l and \mathbf{x}^u , $\mathbf{y} \in \mathcal{Y}$ is the design parameters vector collecting those quantities that are independent of the designer choice (e.g., operating and environmental conditions), f_k with $k = 1, \dots, N_f$ are the N_f objective functions, g_n with $n = 1, \dots, N_g$ are the N_g functional constraints, whereas h_i ($i = 1, \dots, I$) and q_j ($j = 1, \dots, J$) are the inequality and equality design constraints, respectively.

Several sources of uncertainty may affect the problem in Eq. (1):

1. \mathbf{x} is affected by a stochastic error/uncertainty (e.g., tolerance of the design variables);
2. \mathbf{y} is an intrinsic stochastic random process (e.g., the operating and environmental conditions are defined by probability densities);
3. the evaluation of objectives f_k and constraints g_n is affected by errors stemming from modeling and/or computing.

Here, the focus is on the second source of uncertainty, where the probability density function p associated with \mathbf{y} has to be evaluated and/or given somehow. The effects of input uncertainties are considered evaluating the expected value (\mathbb{E}) of the original objective function

$$\mathbb{E}[f(\mathbf{x}, \mathbf{y})] = \int_{\mathcal{Y}} f(\mathbf{x}, \mathbf{y})p(\mathbf{y})d\mathbf{y}, \tag{2}$$

and addressing the constraints as probabilistic inequalities (\mathbb{P}) such as

$$\mathbb{P}[g(\mathbf{x}, \mathbf{y})] = \int_{\mathcal{Y}} \bigcap_{n=1}^{N_g} [g_n(\mathbf{x}, \mathbf{y}) \leq 0] p(\mathbf{y})d\mathbf{y}. \tag{3}$$

The stochastic counterpart of the DDO problem in Eq. (1) can be then formulated as a reliability-based robust design optimization (RBRDO) problem as follows

$$\begin{aligned}
 &\text{minimize } \mathbb{E}[f_k(\mathbf{x}, \mathbf{y})] \\
 &\text{subject to } \mathbb{P}[g(\mathbf{x}, \mathbf{y})] \geq P_0 \\
 &\quad \text{and to } h_i(\mathbf{x}) \leq 0 \\
 &\quad \text{and to } q_j(\mathbf{x}) = 0 \\
 &\quad \text{and to } \mathbf{x}^l \leq \mathbf{x} \leq \mathbf{x}^u,
 \end{aligned} \tag{4}$$

where P_0 is a prescribed minimum reliability associated with the functional constraints. It may be noted that, if necessary, the expected value may be replaced either by the standard deviation or by a weighted sum of expected value and standard deviation.

Here, instead of defining an a priori value for P_0 , the design reliability \mathbb{P} is used as a second objective function and the RBRDO is recast in the multi-objective problem

$$\begin{aligned}
 &\text{minimize } \{ \mathbb{E}[f_k(\mathbf{x}, \mathbf{y})], -\mathbb{P}[g(\mathbf{x}, \mathbf{y})] \}^T \\
 &\quad \text{and to } h_i(\mathbf{x}) \leq 0 \\
 &\quad \text{and to } q_j(\mathbf{x}) = 0 \\
 &\quad \text{and to } \mathbf{x}^l \leq \mathbf{x} \leq \mathbf{x}^u.
 \end{aligned} \tag{5}$$

Once the multi-objective problem is solved and the associated set of non-dominated solutions is identified, the choice is left to the decision maker of the proper trade-off between the minimization of the objective expected value and the maximization of the design reliability.

3 Computational-cost reduction methods

The simple SBDO scheme presented in Fig. 1 is extended to include computational-cost reduction methods, as shown in Fig. 2. Namely, the extended scheme includes: a design-space dimensionality reduction procedure before the optimization loop, UQ methods, and an adaptive metamodel to alleviate both UQ and global optimization procedures. More in details, the computational-cost reduction methods used in the present work (and presented in the following subsections) are: (a) a physics-informed design-space dimensionality reduction by a generalized KLE, (b) an adaptive metamodel based on SRBF, (c) Gaussian quadrature and metamodel-based importance sampling as UQ methods, and finally (d) a global multi-objective optimization algorithm based on a deterministic variant of PSO.

3.1 Physic-informed design-space dimensionality reduction

Consider a geometric domain \mathcal{G} (which identifies the initial or parent shape) and a set of coordinates $\xi \in \mathcal{G} \subset \mathbb{R}^n$ with $n = 1, 2, 3$. Assume that $\mathbf{u} \in \mathcal{U} \subset \mathbb{R}^M$ is the design-variable vector, which defines a continuous shape modification vector $\delta(\xi, \mathbf{u}) \in \mathbb{R}^m$ with $m = 1, 2, 3$ (with m not necessarily equal to

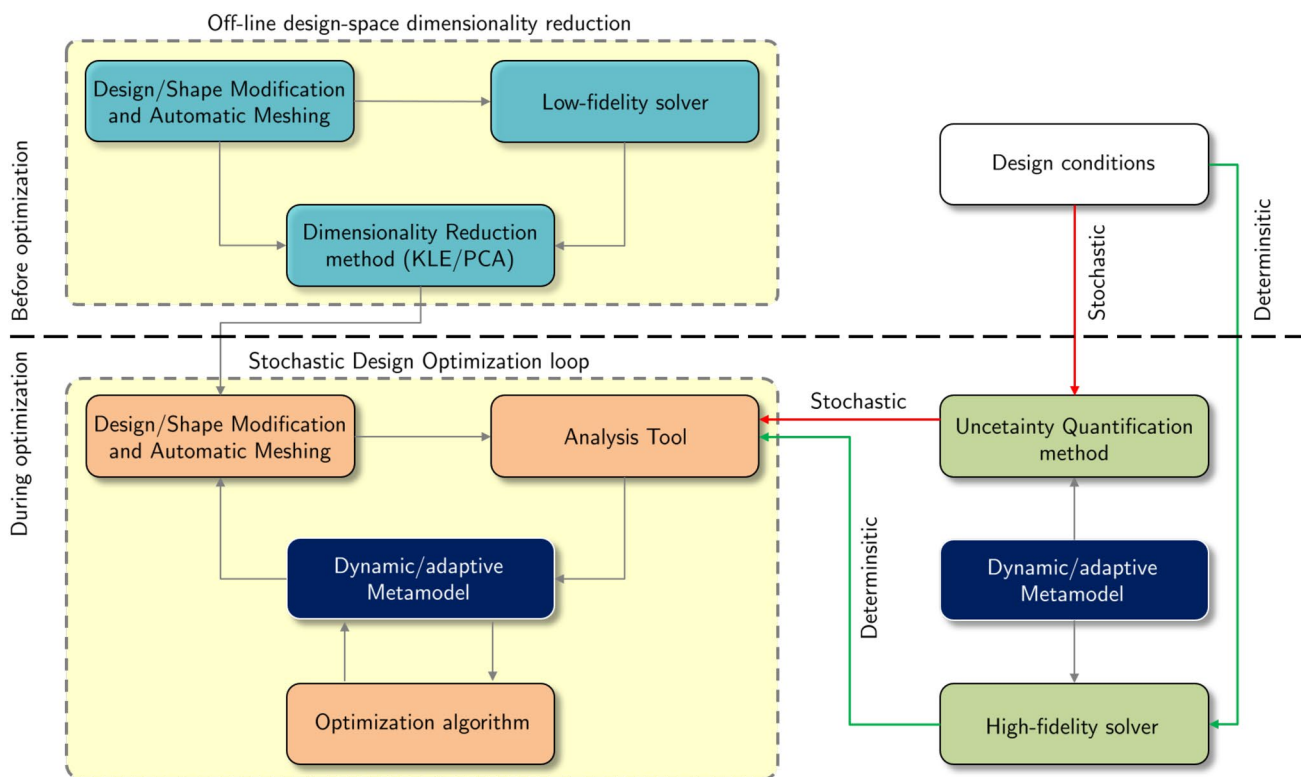


Fig. 2 SBDO scheme using computational-cost reduction methods

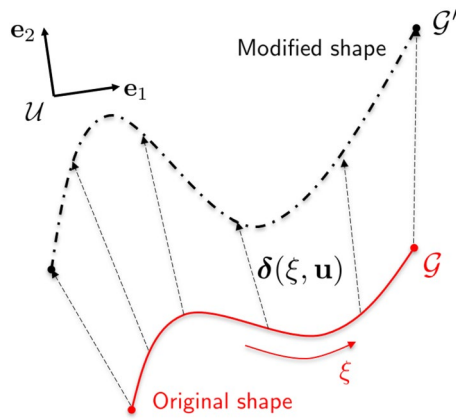


Fig. 3 Geometry modification concept

n), which maps each point to its modified counterpart. Given the shape modification vector, a geometry $\mathbf{g} \in \mathcal{G}$ can be transformed to a deformed geometry $\mathbf{g}' \in \mathcal{G}'$ (see Fig. 3) by computing updated point locations

$$\mathbf{g}'(\xi, \mathbf{u}) = \mathbf{g}(\xi) + \delta(\xi, \mathbf{u}) \tag{6}$$

for each $\xi \in \mathcal{G}$.

Consider the shape modification vector $\delta \in \mathbb{R}^{m_1}$, $m_1 = 1, \dots, 3$, along with a distributed physical parameter vector $\pi \in \mathbb{R}^{m_2}$, $m_2 = 1, \dots, \infty$ (representing, e.g., velocity, pressure distribution, wave elevation, etc.), and a lumped (or global) physical parameter vector $\theta \in \mathbb{R}^{m_3}$, $m_3 = 1, \dots, \infty$ (representing, e.g., ship resistance, motion RMS, etc.).

For the sake of simplicity, consider one set of coordinates $\xi \in \mathbb{R}^n$, and assume \mathcal{G} , \mathcal{P} , and \mathcal{Q} as the domain of δ , π , and θ , respectively, as schematized in Fig. 4. Note that \mathcal{Q} has a null measure and corresponds to an arbitrary point ξ_θ where the lumped physical parameter vector is virtually defined. Also note that, in general, $\mathcal{D} \equiv \mathcal{G} \cup \mathcal{P} \cup \mathcal{Q}$ is not simply connected.

Consider a combined geometry and physics-based vector $\gamma \in \mathbb{R}^m$ with $m = \max\{m_1, m_2, m_3\}$, where the physics can be multi-disciplinary,

$$\gamma(\xi, \mathbf{u}) = \begin{cases} \delta(\xi, \mathbf{u}) & \text{if } \xi \in \mathcal{G} \\ \pi(\xi, \mathbf{u}) & \text{if } \xi \in \mathcal{P} \\ \theta(\xi, \mathbf{u}) & \text{if } \xi \in \mathcal{Q} \end{cases} \tag{7}$$

as belonging to a disjoint Hilbert space $L^2_\rho(\mathcal{D})$, defined by the generalized inner product

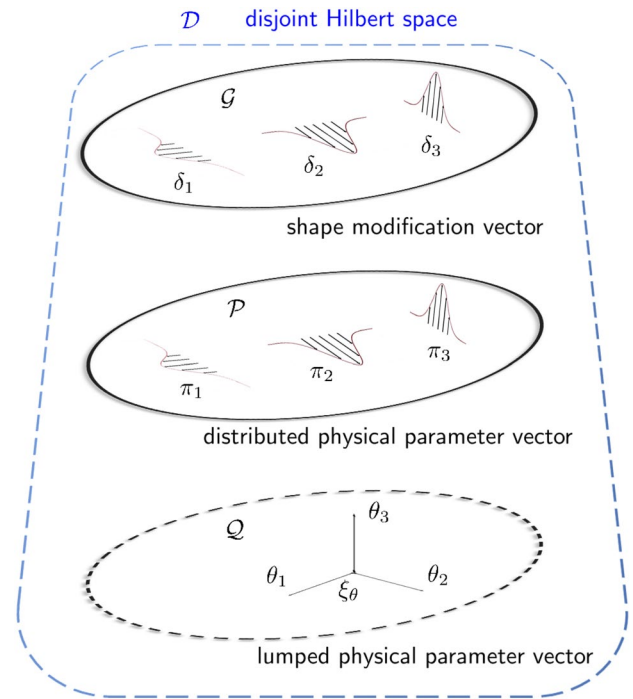


Fig. 4 Domains for shape modification vector, distributed physical parameter vector, and lumped (or global) physical parameter vector in a disjoint Hilbert space

$$\begin{aligned} \langle \mathbf{a}, \mathbf{b} \rangle_\rho &= \int_{\mathcal{D}} \rho(\xi) \mathbf{a}(\xi) \cdot \mathbf{b}(\xi) d\xi \\ &= \int_{\mathcal{G}} \rho(\xi) \mathbf{a}(\xi) \cdot \mathbf{b}(\xi) d\xi \\ &\quad + \int_{\mathcal{P}} \rho(\xi) \mathbf{a}(\xi) \cdot \mathbf{b}(\xi) d\xi \\ &\quad + \rho(\xi_\theta) \mathbf{a}(\xi_\theta) \cdot \mathbf{b}(\xi_\theta) \end{aligned} \tag{8}$$

with associated norm $\|\mathbf{a}\| = (\mathbf{a}, \mathbf{a})_\rho^{\frac{1}{2}}$, where $\rho(\xi) \in \mathbb{R}$ is an arbitrary weight function.

Consider \mathbf{u} as a random variable, with associated probability density function $p(\mathbf{u})$. This corresponds to formulating the optimization problem as a problem affected by epistemic uncertainty, in the sense that before solving the problem, the optimal solution is yet unknown. Once $p(\mathbf{u})$ is defined, considering all possible realizations of \mathbf{u} , the associated mean vector is

$$\langle \gamma \rangle = \int_{\mathcal{U}} \gamma(\xi, \mathbf{u}) p(\mathbf{u}) d\mathbf{u} \tag{9}$$

and the associated variance (combined geometry and physics based variability) equals

$$\sigma^2 = \langle \|\hat{\boldsymbol{\gamma}}\|^2 \rangle = \int_U \int_{\mathcal{D}} \rho(\boldsymbol{\xi}) \hat{\boldsymbol{\gamma}}(\boldsymbol{\xi}, \mathbf{u}) \cdot \hat{\boldsymbol{\gamma}}(\boldsymbol{\xi}, \mathbf{u}) p(\mathbf{u}) d\boldsymbol{\xi} d\mathbf{u}, \quad (10)$$

where $\hat{\boldsymbol{\gamma}} = \boldsymbol{\gamma} - \langle \boldsymbol{\gamma} \rangle$ represent the combined geometry and physics based modification vector, and $\langle \cdot \rangle$ denotes the ensemble average over \mathbf{u} .

The aim of the KLE is to find an optimal basis of orthogonal functions for the linear representation of $\hat{\boldsymbol{\gamma}}$:

$$\hat{\boldsymbol{\gamma}}(\boldsymbol{\xi}, \mathbf{u}) \approx \sum_{k=1}^N x_k(\mathbf{u}) \boldsymbol{\psi}_k(\boldsymbol{\xi}) \quad (11)$$

where, $\boldsymbol{\psi}_k$ is defined as

$$\boldsymbol{\psi}_k(\boldsymbol{\xi}) = \begin{cases} \boldsymbol{\varphi}_k(\boldsymbol{\xi}) & \text{if } \boldsymbol{\xi} \in \mathcal{G} \\ \boldsymbol{\chi}_k(\boldsymbol{\xi}) & \text{if } \boldsymbol{\xi} \in \mathcal{P} \\ \boldsymbol{\nu}_k(\boldsymbol{\xi}) & \text{if } \boldsymbol{\xi} \in \mathcal{Q} \end{cases} \quad (12)$$

and

$$x_k(\mathbf{u}) = (\hat{\boldsymbol{\gamma}}, \boldsymbol{\psi}_k)_\rho = \int_{\mathcal{D}} \rho(\boldsymbol{\xi}) \hat{\boldsymbol{\gamma}}(\boldsymbol{\xi}, \mathbf{u}) \cdot \boldsymbol{\psi}_k(\boldsymbol{\xi}) d\boldsymbol{\xi} \quad (13)$$

are the basis-function components, used hereafter as new (reduced) design variables.

The optimality condition associated to the KLE refers to the geometric and physics-based variance retained by the basis functions through Eq. (11). Combining Eqs. (10)–(13) yields

$$\begin{aligned} \sigma^2 &= \sum_{k=1}^{\infty} \sum_{j=1}^{\infty} \langle x_k x_j \rangle (\boldsymbol{\psi}_k, \boldsymbol{\psi}_j)_\rho \\ &= \sum_{j=1}^{\infty} \langle x_j^2 \rangle = \sum_{j=1}^{\infty} \langle (\hat{\boldsymbol{\gamma}}, \boldsymbol{\psi}_j)_\rho^2 \rangle. \end{aligned} \quad (14)$$

The basis retaining the maximum variance is formed by those $\boldsymbol{\psi}$, solutions of the variational problem

$$\begin{aligned} &\underset{\boldsymbol{\psi} \in L^2_\rho(\mathcal{D})}{\text{maximize}} \quad \mathcal{J}(\boldsymbol{\psi}) = \langle (\hat{\boldsymbol{\gamma}}, \boldsymbol{\psi})_\rho^2 \rangle \\ &\text{subject to} \quad (\boldsymbol{\psi}, \boldsymbol{\psi})_\rho^2 = 1 \end{aligned} \quad (15)$$

which yields [14]

$$\begin{aligned} \mathcal{L}\boldsymbol{\psi}(\boldsymbol{\xi}) &= \int_{\mathcal{D}} \rho(\boldsymbol{\xi}') \langle \hat{\boldsymbol{\gamma}}(\boldsymbol{\xi}, \mathbf{u}) \otimes \hat{\boldsymbol{\gamma}}(\boldsymbol{\xi}', \mathbf{u}) \rangle \boldsymbol{\psi}(\boldsymbol{\xi}') d\boldsymbol{\xi}' \\ &= \lambda \boldsymbol{\psi}(\boldsymbol{\xi}), \end{aligned} \quad (16)$$

where \mathcal{L} is the selfadjoint integral operator whose eigen-solutions define the optimal basis functions for the linear representation of Eq. (11). Therefore, its eigenfunctions (KL

modes) $\{\boldsymbol{\psi}_k\}_{k=1}^{\infty}$ are orthogonal and form a complete basis for $L^2_\rho(\mathcal{D})$. Additionally, it may be proven that

$$\sigma^2 = \sum_{k=1}^{\infty} \lambda_k, \quad (17)$$

where the eigenvalues λ_k (KL values) represent the variance retained by the associated basis function $\boldsymbol{\psi}_k$, through its component x_k in Eq. (11):

$$\lambda_k = \langle x_k^2 \rangle. \quad (18)$$

Finally, the solutions $\{\boldsymbol{\psi}_k\}_{k=1}^{\infty}$ of Eq. (16) are used to build a reduced-dimensionality design space. Defining l , with $0 < l \leq 1$, as the desired confidence level of the DR, N in Eq. (11) is selected such as

$$\sum_{k=1}^N \lambda_k \geq l \sum_{k=1}^{\infty} \lambda_k = l\sigma^2 \quad (19)$$

with $\lambda_k \geq \lambda_{k+1}$. After the design-space DR is assessed and performed, the geometric components $\{\boldsymbol{\varphi}_k\}_{k=1}^N$ of the eigenvectors $\boldsymbol{\psi}_k$ in Eq. (12) are used for the new representation of the shape modification vector. Details with examples about physics-informed DR numerical implementation are given in [50].

It may be noted that the overall methodology is independent of the specific shape modification method, as this is seen as a black box in the dimensionality-reduction process.

3.2 Adaptive metamodel (SRBF)

Consider an objective function $f(\mathbf{x})$. Let the true function value be known in a number N_T of training points \mathbf{x}_j with associated objective function values $f(\mathbf{x}_j)$. The metamodel prediction $\tilde{f}(\mathbf{x})$ is computed as the expected value of an RBF prediction sample (i.e., SRBF [63]) obtained considering a stochastic tuning parameter in the RBF kernel, e.g., $\tau \sim \text{unif}[1, 3]$:

$$\tilde{f}(\mathbf{x}) = \mathbb{E} [g(\mathbf{x}, \tau)]_\tau, \quad (20)$$

with

$$g(\mathbf{x}, \tau) = \sum_{j=1}^{N_T} w_j \|\mathbf{x} - \mathbf{x}_j\|^\tau, \quad (21)$$

where w_j are unknown coefficients, $\|\cdot\|$ is the Euclidean norm. The coefficients w_j can be determined enforcing exact interpolation at the training points $g(\mathbf{x}_j, \tau) = f(\mathbf{x}_j)$ by solving

$$\mathbf{A}\mathbf{w} = \mathbf{f}, \quad (22)$$

where \mathbf{A} is the Gram matrix defined as $\mathbf{A}_{ij} = \|\mathbf{x}_i - \mathbf{x}_j\|^\tau$, $\mathbf{w} = \{w_j\}$, and $\mathbf{f} = \{f(\mathbf{x}_j)\}$.

This ensemble of RBF provides function prediction and associated uncertainty, evaluated using a Monte Carlo sampling over τ [63]. The metamodel can be built with a relatively small-size initial DoE and then dynamically updated by adding samples only where it is most informative, to improve its accuracy.

3.3 Uncertainty quantification methods

The quantitative characterization and reduction of uncertainties of the computational output is here provided by Gaussian quadrature and metamodel-based importance sampling.

3.3.1 Gaussian quadrature

An n -point Gaussian quadrature rule is constructed to yield an exact result for polynomials of degree $2n - 1$ (or lower) by a suitable choice of the points x_i and weights w_i for $i = 1, \dots, n$. The expected value of $f(x)$ is stated as [15]

$$\mathbb{E}[f(x)] = \int_a^b f(x)dx \approx \sum_{i=1}^n w_i f(x_i), \tag{23}$$

Equation (23) can be easily extended to multidimensional integral.

3.3.2 Metamodel-based importance sampling

Importance sampling is a method for estimating expectation [60]. Let $f(\mathbf{x})$ be a known function of a random variable vector \mathbf{x} distributed according to $p(\mathbf{x})$. If it is not possible or convenient to draw samples from $p(\mathbf{x})$. Let $q(\mathbf{x})$ be another distribution from which samples \mathbf{x}_i ($i = 1, \dots, n$) are drawn, then

$$\mathbb{E}[f(\mathbf{x})] \approx \frac{\sum_{i=1}^n w(\mathbf{x}_i) f(\mathbf{x}_i)}{\sum_{i=1}^n w(\mathbf{x}_i)}, \tag{24}$$

with

$$w(\mathbf{x}) := \frac{p(\mathbf{x})}{q(\mathbf{x})}. \tag{25}$$

Equation (24) is applied to the metamodel predictions.

3.4 Multi-objective optimization algorithm (MODPSO)

The PSO algorithm [27] belongs to the class of metaheuristic algorithms for single-objective derivative-free global optimization. It is based on the social-behavior

metaphor of a flock of birds or a swarm of bees searching for food. The original PSO formulation makes use of random coefficients, to enhance the swarm dynamics and variability. This approach might be too expensive in SBDO for real industrial applications, since statistically convergent results can be obtained only through extensive numerical campaigns. Therefore a deterministic PSO has been introduced in [44] and a discussion for its effective and efficient use in SBDO, with comparison to the original (stochastic) PSO has been presented in [52]. The extension of deterministic PSO to a multi-objective formulation (MODPSO) has been proposed in [45] as follows

$$\begin{cases} \mathbf{v}_j^{i+1} = \chi \left[\mathbf{v}_j^i + \phi_1 (\mathbf{p}_j - \mathbf{x}_j^i) + \phi_2 (\mathbf{g}_j - \mathbf{x}_j^i) \right] \\ \mathbf{x}_j^{i+1} = \mathbf{x}_j^i + \mathbf{v}_j^{i+1}, \end{cases} \tag{26}$$

where \mathbf{v}_j^i and \mathbf{x}_j^i are the velocity and the position of the j -th particle at the i -th iteration, χ is the constriction factor, ϕ_1 and ϕ_2 are the cognitive (or personal) and social (or global) learning rates, and \mathbf{p}_j and \mathbf{g}_j are the cognitive and social (personal and global) attractors. Specifically, \mathbf{p}_j is the personal minimizer of an aggregated objective function defined as

$$\mathbf{p}_j = \underset{\mathbf{x}_{p_j}}{\operatorname{argmin}} \sum_{m=1}^M f_m(\mathbf{x}_{p_j}), \quad \text{with} \quad \mathbf{x}_{p_j}^i \in \mathcal{S}_j^i, \tag{27}$$

where $\mathbf{x}_{p_j}^i$ are the points of the personal non-dominated solution set \mathcal{S}_j^i at the i -th iteration, whereas \mathbf{g}_j is the closest point to the j -th particle of the global non-dominated solution set \mathcal{S}^i defined as

$$\mathbf{g}_j = \underset{\mathbf{x}}{\operatorname{argmin}} \|\mathbf{x}_j^i - \mathbf{x}\|, \quad \text{with} \quad \mathbf{x} \in \mathcal{S}^i. \tag{28}$$

A discussion on MODPSO formulations and parameters setup for an effective and efficient use in SBDO has been presented in [41].

4 Hull-form optimization problem

The DTMB 5415 is selected as test case for the current application. The geometry of the DTMB 5415 is shown in Fig. 5. Its main particulars are summarized in Table 1. Since no rudder is considered here, the length between perpendiculars L_{pp} is calculated from the fore perpendicular to the transom bottom edge.

The optimization pertains to the improvement of total resistance and ship operability (or operational effectiveness) in real ocean environment. The flow conditions are representative of realistic operations in the North Atlantic Ocean,

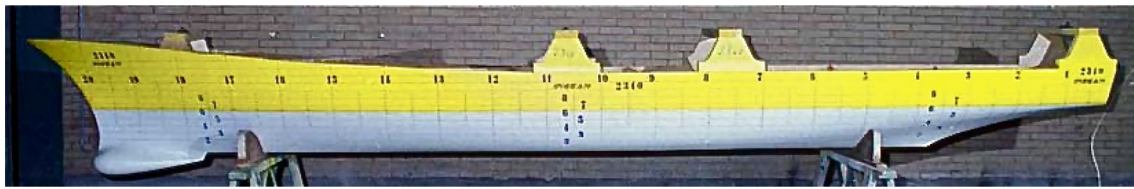


Fig. 5 A geosim replica of the DTMB 5415 (CNR-INSEAN model 2340)

Table 1 DTMB 5415 main particulars and fluid conditions

Description	Symbol	Unit	Full scale	Model scale
Displacement	∇	tonnes	8437	0.549
Length between perpendiculars	L_{pp}	m	142.0	5.720
Beam	B	m	18.90	0.760
Draft	T	m	6.160	0.248
Longitudinal center of gravity	LCG	m	71.60	2.884
Vertical center of gravity	VCG	m	1.390*	0.056*
Bridge longitudinal location	B_x	m	44.00 [†]	1.772 [†]
Bridge vertical location	B_z	m	24.75 [‡]	0.997 [‡]
Flight deck longitudinal location	D_x	m	132.0 [†]	5.317 [†]
Flight deck vertical location	D_z	m	13.00 [‡]	0.524 [‡]
Roll radius of gyration	K_{xx}	–	0.40B	
Pitch radius of gyration	K_{yy}	–	0.25 L_{pp}	
Yaw radius of gyration	K_{zz}	–	0.25 L_{pp}	

★Above the water line

[†]backward bow

[‡]above the keel

considering variable speed, sea state, and heading. The fluid conditions for the numerical simulation are: $\rho = 998.5 \text{ kg/m}^3$, $\nu = 1.09\text{E} - 06 \text{ m}^2/\text{s}$, and $g = 9.8033 \text{ m/s}^2$.

4.1 Problem statement

Two hierarchical SBDO problems are presented from the most general, problem 1 (RBRDO), to the least general, problem 2 (DDO). Problem 1 and 2 details are presented in the following subsections.

4.1.1 Problem 1 (RBRDO)

The following multi-objective RBRDO is solved:

$$\begin{aligned}
 &\text{minimize } \{E[\bar{R}_T(\mathbf{x}, \mathbf{y})], -\Omega(\mathbf{x})\}^T \\
 &\text{subject to } L_{pp}(\mathbf{x}) = L_{pp0}, \\
 &\quad \nabla(\mathbf{x}) = \nabla_0, \\
 &\text{and to } |\Delta B(\mathbf{x})| \leq 0.05B_0, \\
 &\quad |\Delta T(\mathbf{x})| \leq 0.05T_0, \\
 &\quad V(\mathbf{x}) \geq V_0, \\
 &\quad \mathbf{x}_l \leq \mathbf{x} \leq \mathbf{x}_u,
 \end{aligned} \tag{29}$$

with $\mathbf{y} = \{U, H_{1/3}, T_p, \beta\}^T$, where U is the ship speed, $H_{1/3}$ and T_p are the significant wave height and the peak period, respectively, and β is the ship heading (relative to the wave). The objectives in Eq. (29) are the expected value of the (model-scale) mean total resistance ($E[\bar{R}_T]$) in head waves ($\beta = 0$) at variable speed, significant wave height, and peak period and the (full-scale) ship operability (Ω) considering North Atlantic Ocean conditions with variable speed, wave height, peak period, and heading. Finally, inequality and equality geometrical constraints include fixed length between perpendiculars (L_{pp}) and displacement (∇), along with a $\pm 5\%$ maximum variation of beam (B) and draft (T), respectively, and reserved volume V for the sonar in the dome corresponding to 4.9 m diameter and 1.7 m length (cylinder). Subscript ‘0’ indicates original-geometry values. Equality and inequality constraints for the geometry modifications are based on [21].

The objectives are described by Eqs. (30) and (31), respectively

Table 2 Subsystem seakeeping performance criteria [28]

Criterion	Unit	Symbol	SSA*
Roll motion	°	SSA ₁	8.0
Pitch motion	°	SSA ₂	3.0
Vertical acceleration at bridge	g	SSA ₃	0.4
Vertical velocity at flight deck	m/s	SSA ₄	1.98

$$\mathbb{E}[\bar{R}_T(\mathbf{x}, \mathbf{y})] = \int_{\mathbf{y}} \bar{R}_T(\mathbf{x}, \mathbf{y})p(\mathbf{y})d\mathbf{y}, \tag{30}$$

$$\Omega(\mathbf{x}) = \int_{\mathbf{y}} \bigcap_{n=1}^{N_g} [SSA_n(\mathbf{x}, \mathbf{y}) \leq SSA_n^*]p(\mathbf{y})d\mathbf{y}, \tag{31}$$

where p is the joint probability density function of the stochastic operational and environmental parameters; SSA_n are the single significant amplitudes, addressing subsystem seakeeping performance as per NATO STANAG 4154 [28]. These include criteria for mobility, anti-submarine warfare, surface warfare, anti-air warfare, imposing constraints for: roll motion, pitch motion, vertical acceleration at bridge, vertical velocity at flight deck, and wetness/slams/emergences per hour. Here, a limited set of four constraints ($N_g = 4$) is considered, addressing roll and pitch motions, vertical velocity at the flying deck, and vertical acceleration

at the bridge, with maximum allowable values summarized in Table 2.

Stochastic optimization parameters are: speed from 18 to 30 kn ($0.25 \leq Fr \leq 0.41$) following the transit speed–time distribution (see Fig. 6), defined using the kernel density estimation (KDE) of 2013 data from Anderson et al. [1], approximated as

$$p(U) = 2(-0.0063715U + 0.192915); \tag{32}$$

sea state from 4 to 6 following the probability of occurrence for North Atlantic Ocean [2] (see Fig. 6 and Table 3); heading from 0° to 180° following a uniform distribution [28] (see Fig. 6).

Expected mean total resistance in irregular head waves: The time-average total resistance in irregular wave is evaluated by regular wave analysis as

$$\bar{R}_T = R_{CW} + \bar{R}_{AW}, \tag{33}$$

where R_{CW} is the calm-water total resistance and \bar{R}_{AW} is the added resistance, predicted from the non-dimensional added resistance response function (C_{AW}) by

$$\bar{R}_{AW} = 2 \int_0^{+\infty} C_{AW}S_\zeta(\omega_e)d\omega_e, \tag{34}$$

$$C_{AW} = \frac{\bar{R}_{RW} - R_{CW}}{\zeta_0^2}, \tag{35}$$

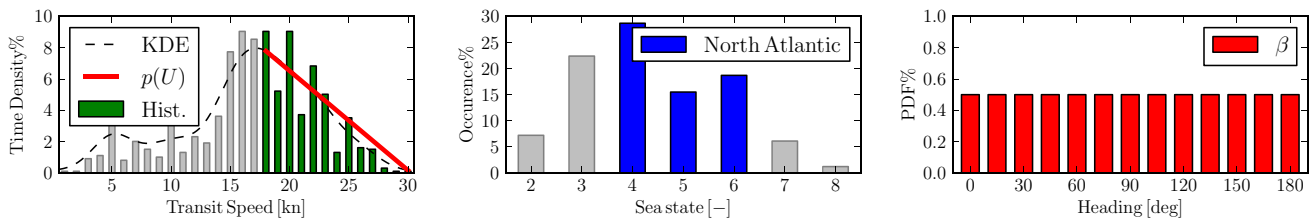


Fig. 6 Stochastic parameters distribution, from left to right: speed U , sea state S , and heading β

Table 3 Annual sea state occurrence in the open North Atlantic Ocean [2]

S	$\hat{p}(S)$ (%)	$p(S)$ (%)	$H_{1/3}$ [m]	$p(H_{1/3})$ (%)	\bar{H} [m]	T_p [s]	ω_a [rad/s]
≤ 1	0.00	–	0.05	–	0.03	–	–
2	7.20	–	0.30	–	0.19	7.5	0.96
3	22.4	–	0.88	–	0.55	7.5	0.96
4	28.7	45.6	1.88	36.5	1.18	8.8	0.81
5	15.5	24.6	3.25	16.4	2.04	9.7	0.74
6	18.7	29.7	5.00	14.9	3.13	12.4	0.58
7	6.10	–	7.50	–	4.70	15.0	0.48
8	1.20	–	11.5	–	7.21	16.4	0.44
> 8	< 0.05	–	> 14	–	> 8.77	20.0	0.36

where ζ_0 is the wave amplitude, ω_e is the wave encounter frequency, and $S_\zeta(\omega_e)$ is the encounter wave spectrum evaluated from the wave spectrum $S_\zeta(\omega)$ as

$$S_\zeta(\omega_e, \mathbf{y}) = S_\zeta(\omega, H_{1/3}, T_p) \frac{g}{g + 2\omega U \cos \beta}, \tag{36}$$

with g the gravity acceleration. Here, the Bretschneider spectrum is considered, defined by

$$S_\zeta(\omega) = \frac{5}{16} \frac{\omega_p^4}{\omega^5} H_{1/3}^2 e^{-5\omega_p^4/4\omega^4}, \tag{37}$$

where $\omega_p = 2\pi/T_p$ is the peak angular frequency. Figure 7 shows the Bretschneider spectra for sea state 4, 5, and 6 for the North Atlantic Ocean (see Table 3).

For the present problem, the mean total resistance expected value is evaluated in head waves only. Defining $\hat{\mathbf{y}} = \{U, H_{1/3}, T_p\}$ and combining Eqs. (33) and (34), Eq. (30) can be recast as

$$\begin{aligned} \mathbb{E}[\bar{R}_T(\mathbf{x}, \hat{\mathbf{y}})] &= \int_U R_{CW}(\mathbf{x}, U) p(U) dU \\ &+ 2 \iint_{U, H_{1/3}} C(\mathbf{x}, U, H_{1/3}) p(U, H_{1/3}) dH_{1/3} dU, \end{aligned} \tag{38}$$

with

$$C(\mathbf{x}, U, H_{1/3}) = \int_{\omega_e} C_{AW}(\mathbf{x}, U, H, \omega_e) S_\zeta(\omega_e, \hat{\mathbf{y}}) d\omega_e \tag{39}$$

where $H = \bar{H}$ is the average height of the Rayleigh distribution evaluated as

$$\bar{H} = \sqrt{\frac{\pi}{8}} H_{1/3}. \tag{40}$$

Operability: The operability (ship-motion related) constraints are related to the SSA of roll ($\hat{\xi}_4$) and pitch ($\hat{\xi}_5$) motions, vertical velocity at the flying deck (v_D), and vertical

acceleration at the bridge (a_B). The SSA of the generic χ -motion is defined as

$$SSA(\chi) = 2\sqrt{m_\chi}, \tag{41}$$

where m_χ is the spectral moment of the generic motion χ . In a probabilistic form the spectral moment m_χ reads

$$m_\chi = \mathbb{E}[q(\omega_e)] = \int_0^{+\infty} q(\omega_e) p(\omega_e) d\omega_e, \tag{42}$$

with

$$q(\omega_e) = m_\zeta \frac{\sigma_\chi^2(\omega_e)}{\zeta_0^2} \quad \text{and} \quad p(\omega_e) = \frac{S_\zeta(\omega_e)}{m_\zeta}, \tag{43}$$

where m_ζ is the area under the encounter wave spectrum

$$m_\zeta = \int_{-\infty}^{+\infty} S_\zeta(\omega_e) d\omega_e, \tag{44}$$

and σ_χ is the standard deviation (STD) or root mean square (RMS, if the signal has zero mean) of the χ -motion, evaluated as

$$\sigma_\chi = \sqrt{\frac{1}{T_2 - T_1} \int_{T_1}^{T_2} [\chi(t) - \bar{\chi}]^2 dt}. \tag{45}$$

Combining Eqs. (41), (42), and (43) with Eq. (31), the latter can be recast as

$$\Omega(\mathbf{x}) = \iiint_{U, H_{1/3}, \beta} \mathcal{B}(\mathbf{x}, \mathbf{y}) p(U, H_{1/3}, \beta) d\beta dH_{1/3} dU, \tag{46}$$

where

$$\mathcal{B}(\mathbf{x}, \mathbf{y}) = \bigcap_{n=1}^{N_g} [\text{SSA}_n(\mathbf{x}, \mathbf{y}) \leq \max(\text{SSA}_n)], \tag{47}$$

with

$$\text{SSA}_n(\mathbf{x}, \mathbf{y}) = 2 \left(\int_0^{+\infty} \frac{\sigma_n^2(\mathbf{x}, U, H, \beta, \omega_e)}{\zeta_0^2} S_\zeta(\omega_e, \mathbf{y}) d\omega_e \right)^{\frac{1}{2}}. \tag{48}$$

4.1.2 Problem 2 (DDO)

Problem 2 represents the deterministic counterpart of problem 1. The following multi-objective deterministic problem is solved:

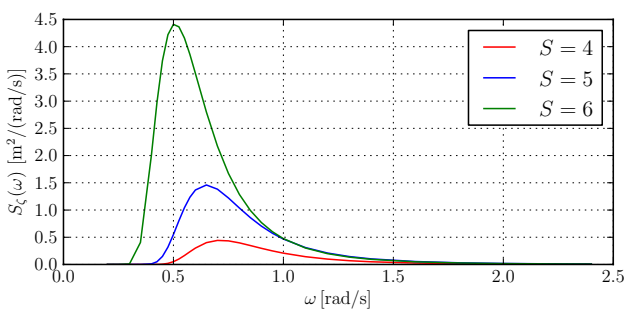


Fig. 7 Bretschneider North Atlantic sea spectra

$$\begin{aligned}
 &\text{minimize } \{\bar{R}_T(\mathbf{x}), \text{SMF}(\mathbf{x})\}^T \\
 &\text{subject to } L_{pp}(\mathbf{x}) = L_{pp0}, \\
 &\quad \nabla(\mathbf{x}) = \nabla_0, \\
 &\quad \text{and to } |\Delta B(\mathbf{x})| \leq 0.05B_0, \\
 &\quad |\Delta T(\mathbf{x})| \leq 0.05T_0, \\
 &\quad V(\mathbf{x}) \geq V_0, \\
 &\quad \mathbf{x}_l \leq \mathbf{x} \leq \mathbf{x}_u,
 \end{aligned} \tag{49}$$

where \bar{R}_T is the mean value of the (model-scale) total resistance in regular head waves at constant speed and wave height, whereas SMF is a seakeeping merit factor based on (full-scale) pitch motion, vertical velocity at flight deck, and vertical acceleration at bridge in head waves and roll motion in quartering ($\beta = 150^\circ$) waves.

Deterministic optimization parameters are: speed equals to 22 kn ($Fr = 0.30$), regular head ($\beta = 0^\circ$) and quartering ($\beta = 150^\circ$) waves, with $\bar{H} = 2.04\text{m}$ and $\omega_a = 0.74\text{rad/s}$, representative of sea state 5. ω_a is the true average frequency [36] evaluated as

$$\omega_a = \frac{2\pi}{T_1}, \quad \text{with } T_1 = 0.772 \left(\frac{5}{3}\right)^{\frac{1}{4}} T_p. \tag{50}$$

Mean total resistance in regular head waves: The time-average total resistance in regular wave is evaluated by

$$\bar{R}_T(\mathbf{x}) = \frac{1}{T_e} \int_0^{T_e} R_T(\mathbf{x}, t) dt \tag{51}$$

with T_e the wave encounter period.

Seakeeping merit factor: The SMF is evaluated by

$$\text{SMF}(\mathbf{x}) = \sum_{n=1}^{N_g} w_n \frac{\sigma_n(\mathbf{x})}{\sigma_{n,0}} \tag{52}$$

where w_n are motion-constraint weights and $\sigma_{n,0}$ are motion-constraint values for the parent hull. Herein, an equal weight of $w_n = 0.25$ is set for $n = 1, \dots, N_g$.

4.2 Design-space definition

Shape modifications are based on a recursive combination of $M = 27$ global modification functions [19] over a hyper-rectangle embedding the demi-hull:

$$\phi_i(\xi) : \mathcal{V} = [0, L_{\xi_1}] \times [0, L_{\xi_2}] \times [0, L_{\xi_3}] \in \mathbb{R}^3 \longrightarrow \mathbb{R}^3, \tag{53}$$

with $i = 1, \dots, M$. Specifically,

$$\delta(\xi, \mathbf{u}) = \delta_M, \tag{54}$$

where

$$\delta_i(\xi, \mathbf{u}) = u_i \phi_i(\xi), \quad \text{with } \begin{cases} \xi = \xi + \delta_{i-1} \\ \delta_1 = 0 \end{cases} \tag{55}$$

The shape modification functions are defined as

$$\phi_i(\xi) := \prod_{j=1}^3 \sin\left(\frac{a_{ij}\pi\xi_j}{L_{\xi_j}} + r_{ij}\right) \mathbf{e}_{q(i)}, \tag{56}$$

where $\{a_{ij}\}_{j=1}^3 \in \mathbb{R}$ define the order of the function along j -th axis; $\{r_{ij}\}_{j=1}^3 \in \mathbb{R}$ are the corresponding spatial phases; $\{L_{\xi_j}\}_{j=1}^3$ are the hyper-rectangle edge lengths; $\mathbf{e}_{q(i)}$ is a unit vector. Modifications are applied along ξ_1 , ξ_2 , or ξ_3 , with $q(i) = 1, 2$, or 3 , respectively. The parameter values used here are taken from [51].

Design space used to solve the optimization problems is defined by the physics-informed DR method [53]. The design variability vector γ of the DR method collects: a (zero-mean) shape modification vector δ based on Eqs. 55, 56; a distributed physical parameter vector π that includes pressure distribution on the hull p and wave elevation η ; and a lumped physical parameter vector θ that includes the wave resistance coefficient in calm water C_w , and the RMS of vertical acceleration at the bridge a_z and pitch angle ξ_5 in waves. Physical parameters vectors are provide by low-fidelity solvers (WARP and SMP), described in the following subsection. The design-space DR is performed considering multiple speeds ($Fr = 0.25, 0.33$, and 0.41), for both calm water and seakeeping performance. The latter are evaluated in head waves at sea state 5 using the Bretschneider spectrum.

The modified geometry is finally built from the reduced-dimensionality space as

$$\mathbf{g}'(\xi, \mathbf{u}) = \mathbf{g}(\xi) + \hat{\delta}(\xi, \mathbf{u}) \tag{57}$$

with

$$\hat{\delta}(\xi, \mathbf{u}) = \sum_{k=1}^N x_k(\mathbf{u}) \boldsymbol{\varphi}_k(\xi), \tag{58}$$

where $\{\boldsymbol{\varphi}_k(\xi)\}_{k=1}^N$ are the geometric component eigenvectors of Eq. (12), and $-\sqrt{3\lambda_k} \leq x_k \leq \sqrt{3\lambda_k}$ are the new design variables and their bounds.

4.3 Hydrodynamic solvers

Characteristics and setups of the flow solvers used for the preliminary design-space DR and the optimization problems are described in the following.

4.3.1 Unsteady Reynolds-averaged Navier–Stokes (URANS) solver

The URANS code CFDSHIP-Iowa [24] is used as high-fidelity solver for the evaluation of the ship resistance in regular waves. CFDSHIP-Iowa V4.5 is an incompressible RANS/DES code, developed at the University of Iowa (IIHR-Hydroscience and Engineering) over the past 30 years, specifically designed for ship hydrodynamics. The equations are solved in an inertial coordinate system, either fixed to a ship or other frame moving at constant speed or in the earth system. The free-surface is modeled with a single-phase capturing approach, meaning that only the water flow is solved, enforcing kinematic and dynamic free-surface boundary conditions on the interfaces. Arbitrary free-surface topologies can be predicted, with the limitation that pressurized closed air/water packets (bubbles) cannot be simulated. It uses structured multiblock grids, and has overset capabilities. Capabilities include 6DoF motions, several turbulence models, moving control surfaces, multi-objects, advanced controllers, propulsion models, incoming waves and winds, bubbly flow, and fluid–structure interaction [39].

In the present study, the URANS equations are solved in the ship coordinate system. The turbulence is computed by the isotropic Menter’s blended $k - \omega/k - \epsilon$ (BKW) model with shear stress transport (SST). A second-order upwind scheme is used to discretize the convective terms of momentum equations. Pressure implicit with splitting of operators (PISO) loop for pressure/velocity coupling is used. For a high-performance parallel computing, an MPI-based domain decomposition approach is used, where each decomposed block is mapped to one processor. The code SUGGAR runs as a separate process from the flow solver to compute interpolation coefficients for the overset grid, which enables CFDSHIP-Iowa to take care of 6DoF with a motion controller at every time step. Simulations are performed for the

right demi-hull for both calm-water and head waves, taking advantage of symmetry about the xz -plane (see Fig. 8).

Figure 8 shows the boundary conditions for calm water/regular wave URANS simulations. The computational domain is composed by a background and a boundary layer volume grid. The background is defined within $0.5L_{pp}$ upstream, $2L_{pp}$ downstream, $2L_{pp}$ sideways, $1.7L_{pp}$ and $0.3L_{pp}$ below and above the waterline, respectively. One volume grid triplet (G1, G2, and G3) is used for calm-water and regular head waves grid verification, with a refinement ratio equal to $\sqrt{2}$, as summarized in Table 4. The boundary layer volume grid is designed to have $0.3 \leq y^+ \leq 0.5$ in the range $0.25 \leq Fr \leq 0.41$, avoiding the use of wall functions, since y^+ is in the viscous sub-layer. The computational domain and G1 grids are shown in Fig. 9.

The verification and validation of the URANS simulations for the original model scale hull in calm water are shown in Fig. 10 (left side) versus the experimental fluid dynamic (EFD) data collected at CNR-INM [40], showing a good agreement. Error bars indicate the grid convergence index uncertainty (U_{GCI}), evaluated using the factor of safety method [64]. Total resistance coefficient, sinkage, trim, and total resistance are found monotonic convergent.

The verification of the URANS simulations for the original model-scale hull in regular head wave, under the DDO problem conditions, is shown in Fig. 10 (right side). The results are found monotonic convergent for the total resistance mean value and the deck vertical velocity standard deviation, whereas the pitch and the bridge vertical acceleration are oscillatory convergent.

4.3.2 Potential flow solvers

The Wave Resistance Program (WARP) is a linear potential flow code developed at CNR-INM. Herein, WARP is used for the evaluation of the calm-water performance for the off-line assessment and dimensionality reduction of the original

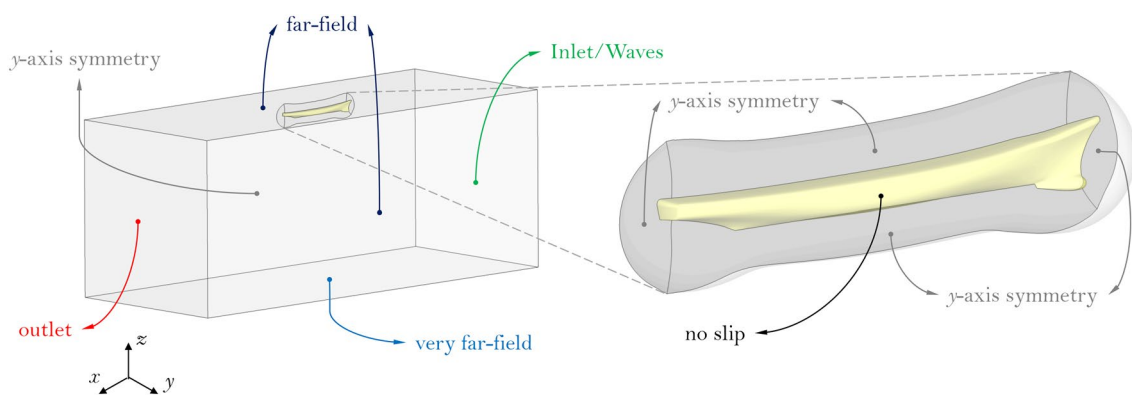


Fig. 8 Summary of boundary conditions for calm water/regular head wave simulations by CFDSHIP-Iowa

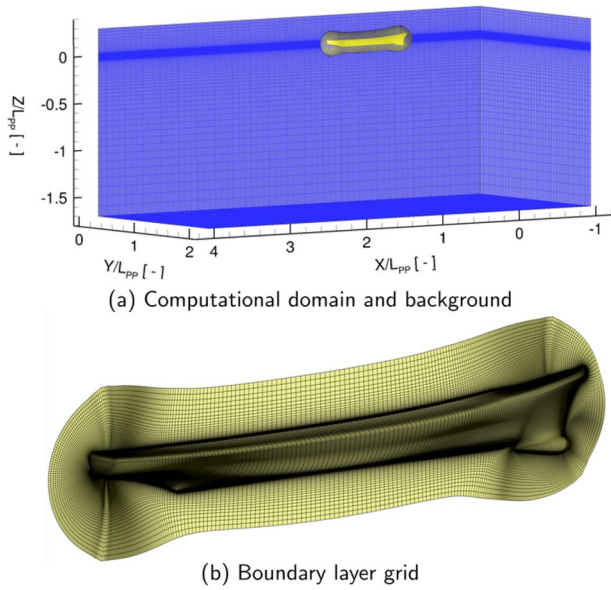


Fig. 9 Computational volume grid used for URANS equations solution (CFDShip-Iowa)

design space (see top-left block in Fig. 2). Wave resistance computations are based on the Dawson (double-model) linearization [10]. The wave resistance is evaluated with the pressure integral over the body surface, whereas the frictional resistance is estimated using a flat-plate approximation, based on the local Reynolds number [49]. The steady 2DoF (sinkage and trim) equilibrium is achieved by iteration of the flow solver and the rigid-body equation of motion. Details of equations, numerical implementations, and validation of the numerical solver are given in [3].

Calm-water potential flow simulations are performed for the right demi hull (composed by 90×25 grid nodes), taking advantage of symmetry about the xz -plane. The computational domain for the free-surface is defined within $1L_{pp}$ upstream, $3L_{pp}$ downstream, and $1.5L_{pp}$ sideways, for a total of 75×20 grid nodes. The computational domain and grids (totally 3.9k nodes) are shown in Fig. 11.

Seakeeping performance are evaluated by the Standard Ship Motion program (SMP), developed at the David Taylor Naval Ship Research and Development Center [34]. SMP provides a potential flow solution based on linearized strip theory. The 6DoF response of the ship is given, advancing at constant forward speed with arbitrary heading in both regular waves and irregular seas, as well as the longitudinal, lateral, and vertical responses at specified locations of the ship.

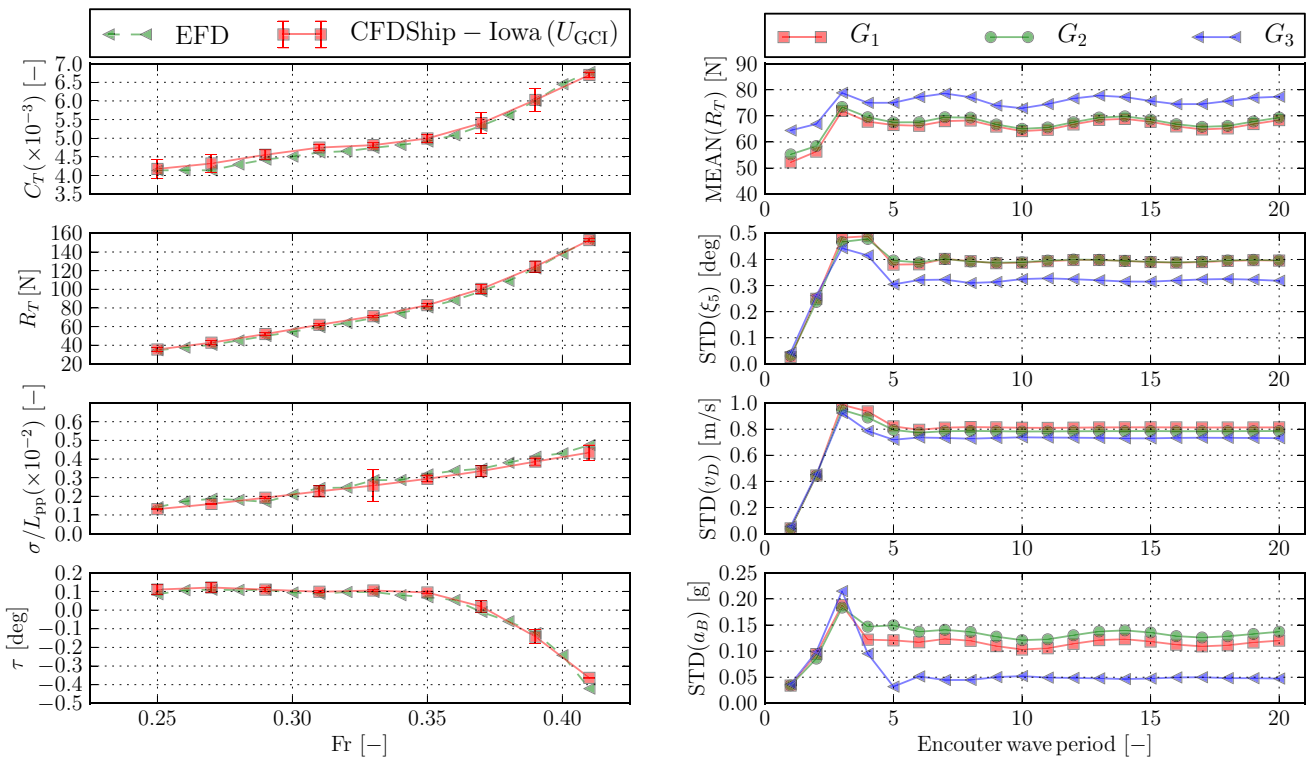


Fig. 10 URANS verification and validation: (left) original hull grid in calm water versus INSEAN experimental (EFD) data; (right) original hull grid in regular wave at deterministic conditions

Table 4 Volume grids used for URANS simulations verification and validation

Grid	r^* ratio	Background	Boundary layer	Total (M)
G1	$\sqrt{2}$	$300 \times 100 \times 150$	$243 \times 71 \times 115$	6.5
G2		$212 \times 71 \times 106$	$172 \times 50 \times 81$	2.3
G3		$150 \times 50 \times 75$	$122 \times 36 \times 58$	0.8

*Refinement ratio

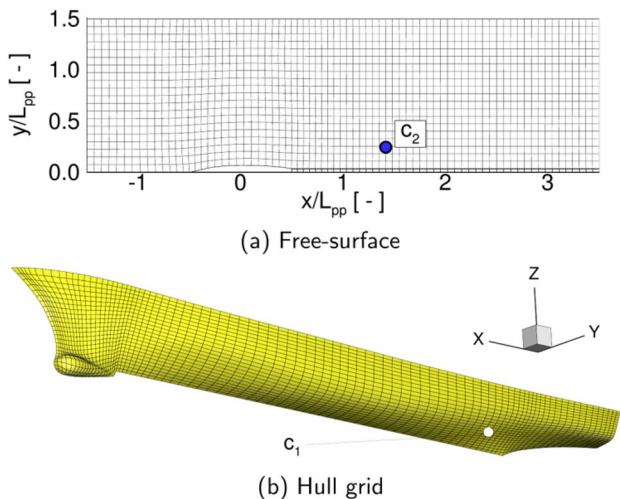


Fig. 11 Computational grids used by the potential flow code for the physics-informed DR method

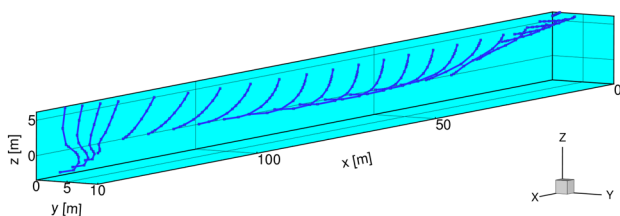


Fig. 12 Computational strip used for linear strip theory and physics-informed DR analysis

Linearized strip theory potential flow simulations are performed for the right demi hull, taking advantage of symmetry about the xz -plane. The computational strips are shown in Fig. 12, each one is discretized with uniformly distributed nodes along the strip curvilinear coordinate. One grid (strips and nodes) triplet (G1, G2, and G3) is used for the seakeeping verification, with a refinement ratio equal to $\sqrt{2}$, as summarized in Table 5.

The solver validation versus the EFD data collected at the IIHR [32] is depicted in Fig. 13, showing a reasonable agreement. Moreover, Fig. 14 compares heave and pitch response amplitude operator obtained by SMP and CFDShip-Iowa for

Table 5 Strips used for seakeeping verification and validation and physics-informed DR simulations

Grid	Refinement ratio	Strips	Nodes	Total
G1	$\sqrt{2}$	31	10	310
G2		22	7	154
G3		16	5	84

the deterministic regular head wave. Linearized strip theory and URANS are almost coincident. This justifies the use of SMP for the evaluation of the seakeeping performance into the optimization procedure, presented in the following subsections.

4.4 Stochastic radial-basis function setup

SRBF metamodel prediction is given as the expectation of 100 RBF metamodels with a power law kernel and stochastic kernel parameter $\tau \sim \text{unif}[1, 3]$.

A full-factorial combination of $N_T = 3^N$ training points is used as initial DoE for the design-variable space. The DoE is then updated adding selected Pareto solutions of the multi-objective optimization problems until convergence.

4.5 Uncertainty quantification setup

UQ method setups for the solution of problems 1 and 2 are described in the following subsections.

4.5.1 Gaussian quadrature for resistance expectation

Gauss–Legendre quadrature with $n = 2$ for each stochastic variable (weights $w_i = 1$ and Gauss points $x_{1,2} = \pm 1/\sqrt{3}$, in normalized coordinates) is used to approximate Eq. (38) as

$$\begin{aligned} \mathbb{E}[\bar{R}_T(\mathbf{x}, \hat{\mathbf{y}})] &\approx \frac{U^u - U^l}{2} \sum_{i=1}^n R_{CW}(\mathbf{x}, U_i) p(U_i) \\ &+ \frac{(U^u - U^l) (H_{1/3}^u - H_{1/3}^l)}{4} \\ &\cdot \sum_{i=1}^n \sum_{j=1}^n \bar{R}_{AW}(\mathbf{x}, U_i, H_{1/3,j}) p(U_i, H_{1/3,j}) \end{aligned} \tag{59}$$

with

$$\begin{aligned} \bar{R}_{AW}(\mathbf{x}, U_i, H_{1/3,j}) &\approx \left(\omega_{e,ij}^u - \omega_{e,ij}^l \right) \sum_{k=1}^n C_{AW}(\mathbf{x}, U_i, \bar{H}_j, \omega_{e,ijk}) S_{\xi,ijk}. \end{aligned} \tag{60}$$

The corresponding Gauss points selected for the URANS simulations are summarized in Table 6.

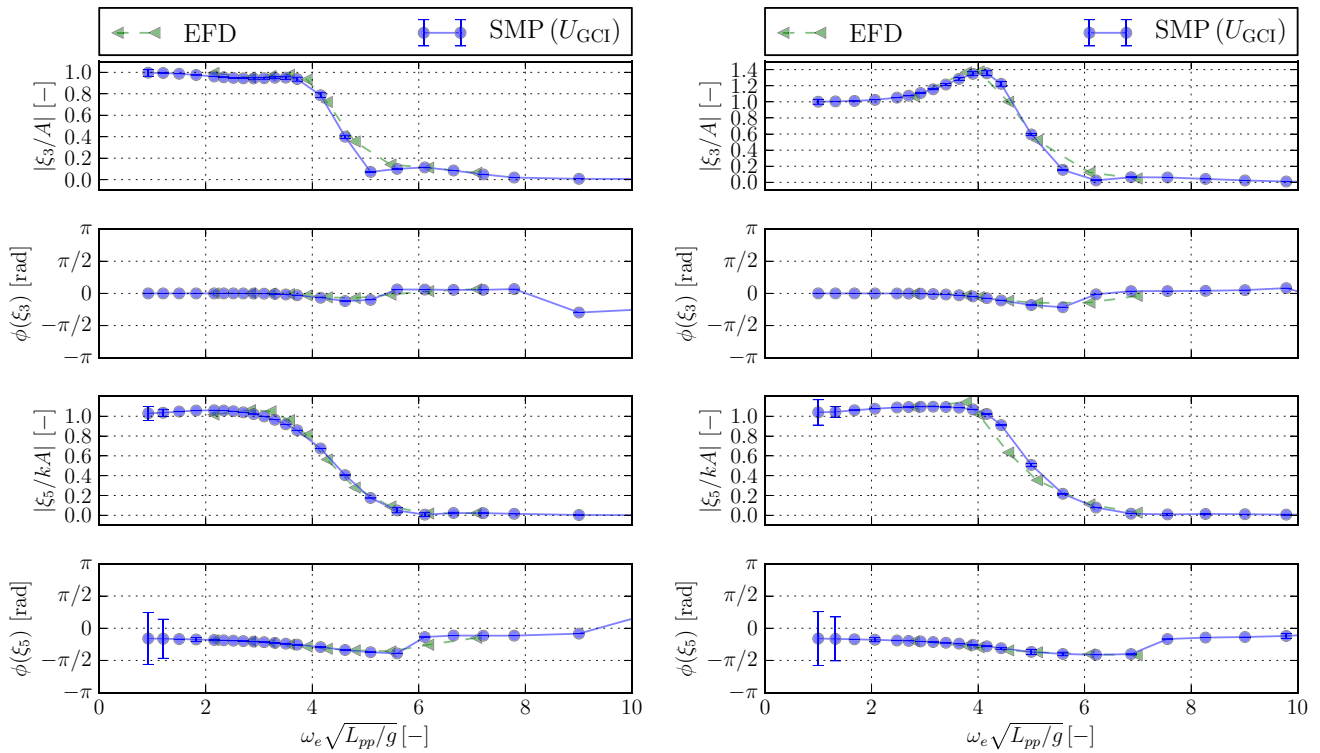


Fig. 13 Seakeeping SMP full scale validation in head waves, in terms of heave ($\hat{\xi}_3$) and pitch ($\hat{\xi}_5$) motion transfer functions versus EFD data: (left) 20 kn, $Fr = 0.28$; (right) 30 kn, $Fr = 0.41$

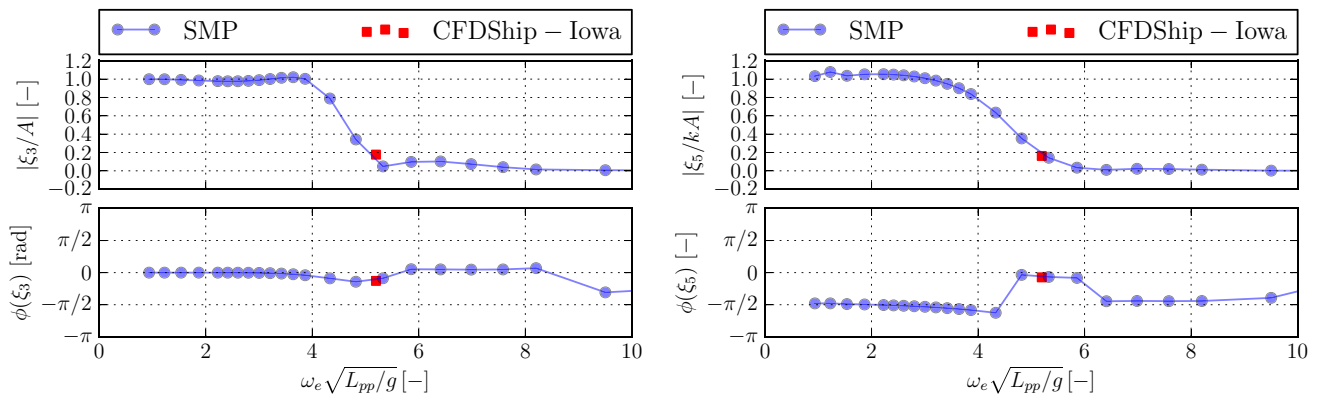


Fig. 14 Comparison of CFDShip-Iowa and SMP on motion transfer functions amplitude and phase for the original DTMB 5415 at 22kn ($Fr = 0.30$): (left) heave; (right) pitch

4.5.2 Metamodel-based importance sampling for operability

A SRBF metamodel is also used for the prediction of the motions SSA (\widetilde{SSA}) and defined as the expected value of 100 RBF metamodels. The motion constraints are evaluated by SMP at the training point, given by the full factorial combination of speeds (uniformly distributed from 18

to 30 kn every 2 knots), significant wave heights equal to 1.88, 3.25, and 5.00 m, and heading spanning from head ($\beta = 0^\circ$) to following ($\beta = 180^\circ$) waves every 2° , for a total of $N_T = 273$.

The operability (Eq. 46) is evaluated by importance sampling and a uniform distribution of items using the SRBF prediction as

Table 6 Stochastic variables used as Gauss points for the solution of problem 1 (RBRDO)

Gauss index			Speed			Sea state				
<i>i</i>	<i>j</i>	<i>k</i>	<i>U</i> [kn]	Fr [–]	Re [–]	<i>H</i> _{1/3} [m]	\bar{H} [m]	<i>T</i> _{<i>p</i>} (<i>H</i> _{1/3}) [s]	ω [rad/s]	ω_e [rad/s]
1	1	1	20.5	0.283	1.11E+7	2.254	1.412	8.80	0.500	0.769
1	1	2	20.5	0.283	1.11E+7	2.254	1.412	8.80	0.770	1.389
1	2	1	20.5	0.283	1.11E+7	4.996	3.131	12.4	0.390	0.611
1	2	2	20.5	0.283	1.11E+7	4.996	3.131	12.4	0.670	1.268
2	1	1	27.5	0.379	1.49E+7	2.254	1.412	8.80	0.560	0.890
2	1	2	27.5	0.379	1.49E+7	2.254	1.412	8.80	0.780	1.410
2	2	1	27.5	0.379	1.49E+7	4.996	3.131	12.4	0.405	0.632
2	2	2	27.5	0.379	1.49E+7	4.996	3.131	12.4	0.710	1.425

$$\Omega(\mathbf{x}) \approx \frac{\sum_{i=1}^{N_U} \sum_{j=1}^{N_{H_{1/3}}} \sum_{k=1}^{N_\beta} \text{SSA}_{ijk}(\mathbf{x}) p(U_i, H_{1/3,j}, \beta_k)}{\sum_{i=1}^{N_U} \sum_{j=1}^{N_{H_{1/3}}} \sum_{k=1}^{N_\beta} p(U_i, H_{1/3,j}, \beta_k)} \quad (61)$$

with

$$\text{SSA}_{ijk}(\mathbf{x}) = \bigcap_{n=1}^{N_g} [\widetilde{\text{SSA}}_n(\mathbf{x}, U_i, H_{1/3,j}, \beta_k) \leq \max(\text{SSA}_n)], \quad (62)$$

where $N_U = N_{H_{1/3}} = N_\beta = 25$.

4.6 Multi-objective deterministic particle swarm optimization setup

A memory-based formulation of MODPSO is used. The suggested optimal parameter setup proposed in [41] is used: eight particles times the number of variables times the number of objectives; particle initialization with Hammersley sequence sampling distribution on domain and bounds with non-null velocity [5]; set of coefficients proposed in [6], i.e., $\chi = 0.721$, $c_1 = c_2 = 1.655$; semi-elastic wall-type approach [55] for box constraints. A linear penalty function is used for the designs exceeding the inequality constraints, $f_m(\mathbf{x}, \mathbf{y}) = f_m(\mathbf{x}, \mathbf{y}) + 100 \sum_{i=1}^I \max\{0, h_i\}$. Equality constraints are satisfied by automatic geometry scaling. A limit to the number of problem evaluations is set equal to 9000, where one problem evaluation collects the evaluation of each objective function. Optimization is performed on the metamodel.

The current MODPSO code is available at <https://www.github.com/MAORG-CNR-INM/POT>.

5 Numerical results

Preliminary design-space assessment and dimensionality reduction results and multi-objective hull-form optimization outcomes are presented in the following subsection.

5.1 Design-space dimensionality reduction

For the current analysis, vectors are normalized so as the variance associated to geometry, distributed and lumped physics parameters is the same (namely, it equals 1). This is a standard approach in machine learning and is done with the evident purpose of properly combining in the data matrix heterogeneous variables, without introducing a bias in favor of any of the quantities under investigation. The normalization also allows for properly assessing small geometric variations that produce large effects on the physical variables. Finally, hull grid nodes below the water line have a weight $\rho(\xi) = 1$, the others $\rho(\xi) = 0$.

Figure 15 shows the KLE results in terms of design variability associated with a reduced-dimensionality space of dimension *N* for *S* = 2250, 4500, and 9000 samples. The results are found convergent versus *S*. The choice of the proper design-space dimensionality is certainly a critical factor to the success of the shape optimization procedure. It may be noted that the definition of the initial shape parameterization can include a large number of design variables and a large variability associated to each variable. The design-space dimensionality reduction is then used to select the most convenient (or reasonable) compromise between design-space dimensionality and associated variability. In this regard, one may say that all choices given by the KLE are to some extent optimal in the Pareto sense (as they minimize the dimensionality while maximize the variability). Here, the following trade-off between design-space dimensionality and variability has been selected. Namely, the RBRDO (problem 1) and DDO (problem 2) are solved

using the first three reduced variables, which resolve about the 65% of the original design variability (see Fig. 15). The corresponding eigenvectors are shown in Fig. 16 (left), where the magnitude of the geometric eigenvector component is depicted, showing the corresponding shape modification. Furthermore, Fig. 16 (right) shows the eigenvectors obtained using a design-space dimensionality reduction procedure based only on geometrical information [14]. It can be noted how the use of physical information affects the shape of the eigenvector geometric component, producing sensibly different reduced-design spaces [17].

5.2 Optimization problems

Optimization results of the RBRDO problem and its deterministic counterpart (DDO) are presented in the following subsections. Table 7 summarizes the problems statements.

A preliminary sensitivity analysis is performed for both RBRDO and DDO problems. Irregular wave total resistance expected value and operability are shown in Fig. 17. Regular wave total resistance and seakeeping merit factor are shown in Fig. 18. RBRDO and DDO problems show potential improvements for both the objectives, even if the objectives are found conflicting.

5.2.1 Problem 1 (RBRDO)

Figure 19 (top) shows the non-dominated solutions set provided by the optimization algorithm in solving Eq. (29). No compromise solutions (capable of improving both the objective) are found, since the objective are completely conflicting. Two designs optima are identified at the extrema (A and B) of the non-dominated solutions set and the corresponding hull stations are shown in Fig. 19 (bottom). Total resistance expected value and operability improvement verification (by CFDShip-Iowa and SMP simulations, respectively) are shown in Fig. 20: design A provides about 3% improvement of the irregular wave total resistance expected value with about 4.8% operability worsening; design B shows 19% worsening of the irregular wave total resistance expected value and about 7.5% operability improvement.

5.2.2 Problem 2 (DDO)

Figure 21 (top) shows the non-dominated solutions set provided by the optimization algorithm in solving Eq. (49). As for the RBRDO, no compromise solutions (capable of improving both the objective) are found. Two designs optima are identified at the extrema (A and B) of the

Table 7 Problem statements summary

Problem	Objectives (symbol)	Flow model (solver)	Ship scale	Fr [-]	U [kn]	$H_{1/3}$ [m]	ω [rad/s]	β [°]
1 (RBRDO)	Mean total Resistance expected Value ($E[\bar{R}_T]$)	URANS (CFDShip-Iowa)	Model	0.25 ÷ 0.41	18.0 ÷ 30.0	1.25 ÷ 6.00	0.39 ÷ 0.78	0
	Operability (Ω)	Linearized strip Theory (SMP)	Full	0.25 ÷ 0.41	18.0 ÷ 30.0	1.25 ÷ 6.00	0.25 ÷ 2.50	0 ÷ 180
2 (DDO)	Mean total Resistance (\bar{R}_T)	URANS (CFDShip-Iowa)	Model	0.30	22.0	3.25	0.74	0
	Seakeeping merit Factor (SMF)	Linearized strip Theory (SMP)	Full	0.30	22.0	3.25	0.74	0; 150

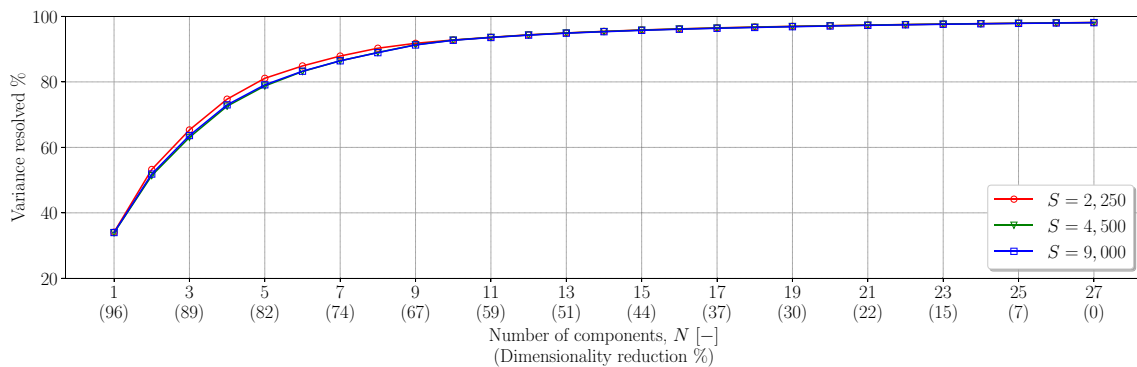


Fig. 15 Variance resolved by reduced-dimensionality space of dimension N

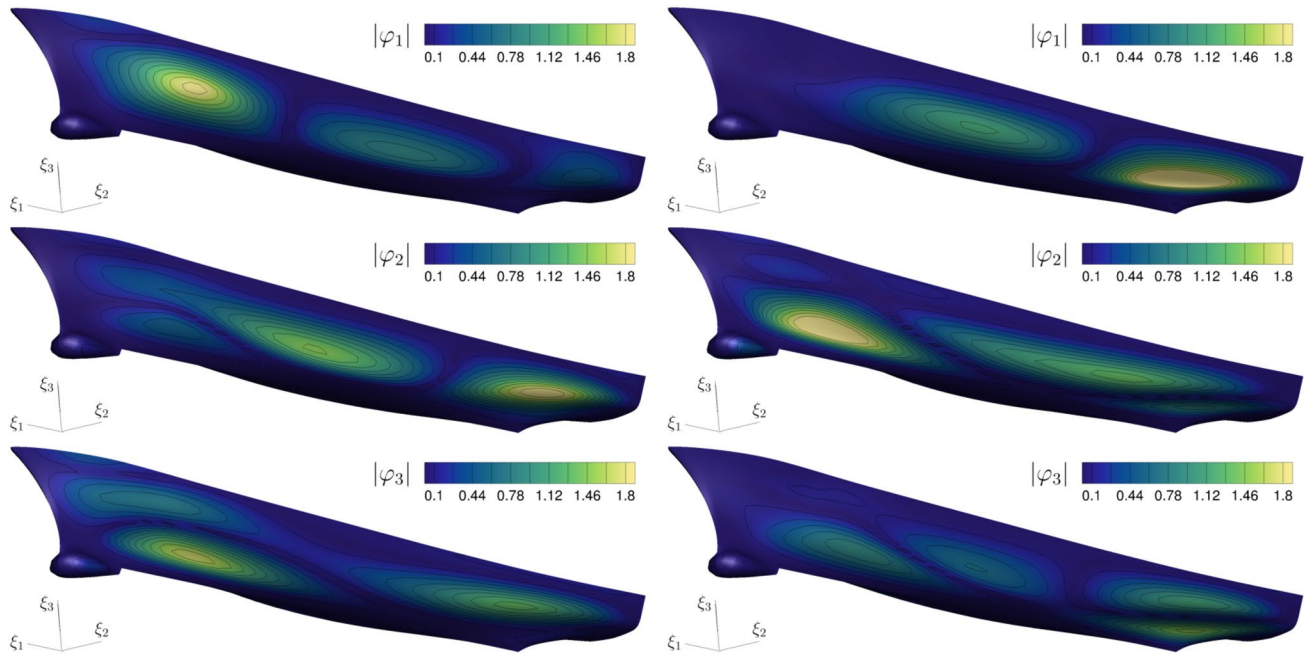


Fig. 16 Magnitude of the first three (ordered from top to bottom) KLE geometric eigenvector component: (left) physics-informed eigenvector used as shape modification basis functions of the reduced-dimensionality design space, (right) geometry-based only eigenvector for comparison

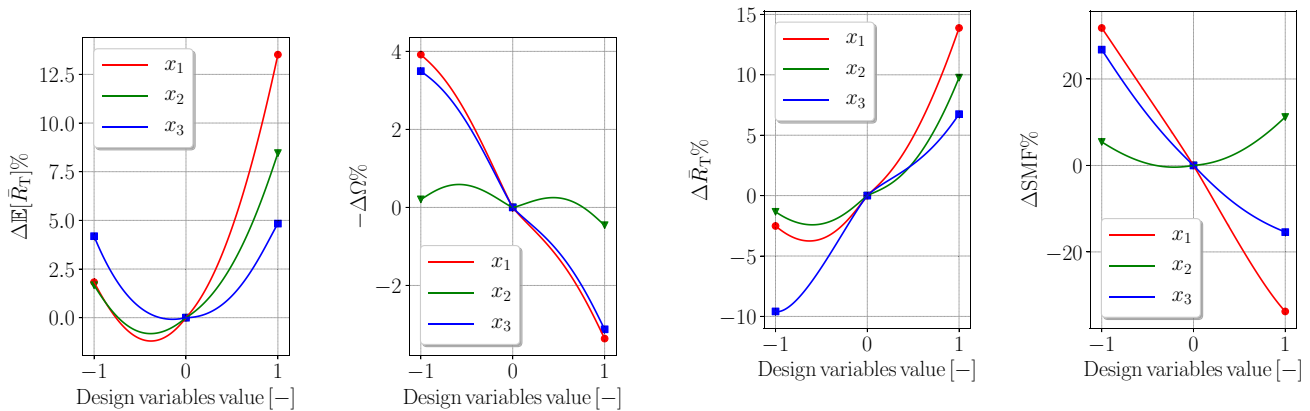


Fig. 17 RBRDO preliminary sensitivity analysis: (left) expected mean total resistance in irregular head waves; (right) operability

Fig. 18 DDO preliminary sensitivity analysis: (left) mean total resistance in regular head waves; (right) seakeeping merit factor

non-dominated solutions set and the corresponding hull stations are shown in Fig. 21 (bottom). Regular-wave total resistance and SMF improvement verification (by CFD-SHIP-Iowa and SMP simulations, respectively) is shown in Fig. 22: design A provides about 5.4% improvement of the regular-wave total resistance with about 27% SMF worsening; design B shows about 19% worsening of the regular-wave total resistance and 36.5% SMF improvement.

6 Discussion

RBRDO and DDO results show similar trends of the optimization procedure. No compromise solutions is found for both problems, even if a significant improvement of all the objectives is found at the extrema of both RBRDO and DDO non-dominated solutions sets. Stochastic (RBRDO) and deterministic (DDO) optimal designs improvements and cross-verification results are summarized in Table 8. As expected, the deterministic optima are worse than stochastic in the stochastic conditions and vice versa.

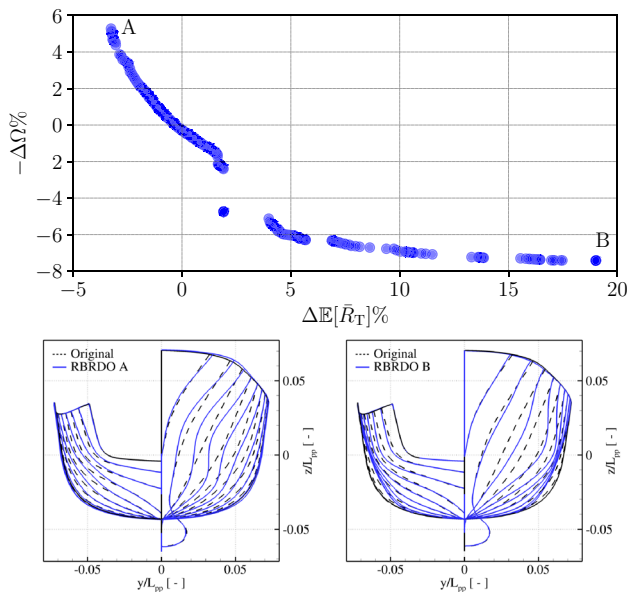


Fig. 19 RBRDO non-dominated solutions set (top) and optimum designs (bottom)

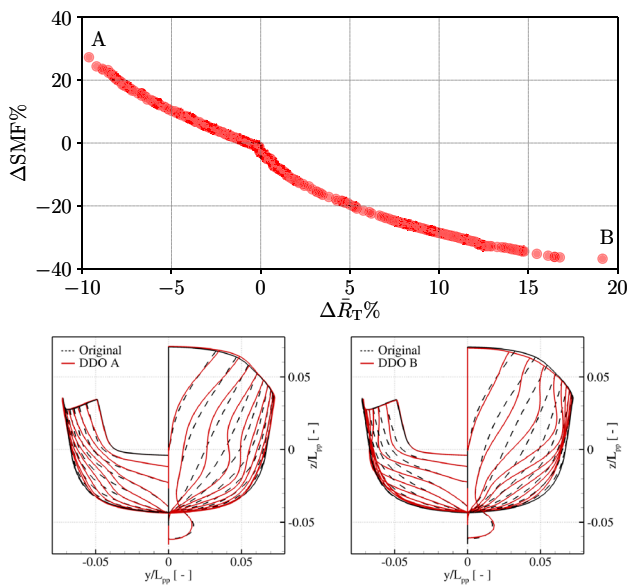


Fig. 20 RBRDO optima verification: $\tilde{\sim}$ represents the metamodel prediction

Table 8 Deterministic and stochastic design optimization summary

Problem	Objective	Original	Optima* [†] (Δ%)			
			RBRDO (A)	RBRDO (B)	DDO (A)	DDO (B)
1 (RBRDO)	$E[\bar{R}_T]$ [N]	62.43	- 2.77	19.0	3.44	13.3
	$-\Omega\%$	- 71.90	4.82	- 7.42	3.56	- 6.31
2 (DDO)	\bar{R}_T [N]	67.70	- 4.92	30.8	- 5.43	19.2
	SMF [-]	1.000	69.6	- 10.5	27.3	- 36.5

★Bold face indicates desired objective (resistance or seakeeping/operability)

†Italics indicate cross-verification results

Nevertheless, RBRDO optima provide improvements also at deterministic conditions, while the same cannot be said for the deterministic optima. A deeper comparison at the deterministic conditions of the RBRDO and DDO optima is conducted via URANS verification. Figure 23 compares the hull stations of the optimal designs A and B, showing the differences between the stochastic and deterministic optimal hull. Furthermore, Table 9 provides a comparison of these geometries in terms of calm water and regular-wave performance, including added resistance, and RMS of heave, pitch, vertical velocity at the flight deck, and acceleration at the bridge, and finally the relative motion (RM) of the ship bow to the free surface. Designs A provides the most interesting results. RBRDO A shows a resistance improvement in both calm water (-4.7%) and regular waves (-4.9%), as well as a remarkable improvement (-5.9%) of the added resistance with an associated reduction of the RM at the bow (-1.5%). Motions' RMS are reasonable, but the acceleration at the bridge. It may be noted how, as expected, designs A show a significant reduction of the resistance in waves, whereas designs B present significant reduction of the motions' RMS. .

Original calm-water free-surface (see Fig. 24 first line) is compared to RBRDO (A and B in Fig. 24 second and third lines, respectively) and DDO (A and B in Fig. 24 fourth and fifth lines, respectively) optima at different speeds ($Fr = 0.283, 0.300, \text{ and } 0.379$ in Fig. 24 from left to right), where $Fr = 0.3$ corresponds to the deterministic speed, while $Fr = 0.283$ and 0.379 correspond to the Gaussian coordinates used for stochastic optimization. Designs A reduce the wave elevation, especially for the stern diverging Kelvin waves, whereas designs B are obviously worse than the original.

Heave, roll, and pitch transfer functions comparison of original, RBRDO, and DDO designs at the deterministic optimization conditions ($\beta=0^\circ$ for heave and pitch and 150° for roll at $Fr = 0.30$) is provided in Fig. 25. RBRDO and DDO designs B show reduced transfer functions than the original, specially for heave and roll motions, whereas designs A are increased; no significant differences are found for the pitch motion.

Finally, a comparison of the optimal design variable values is provided in Fig. 26. RBRDO design B and DDO

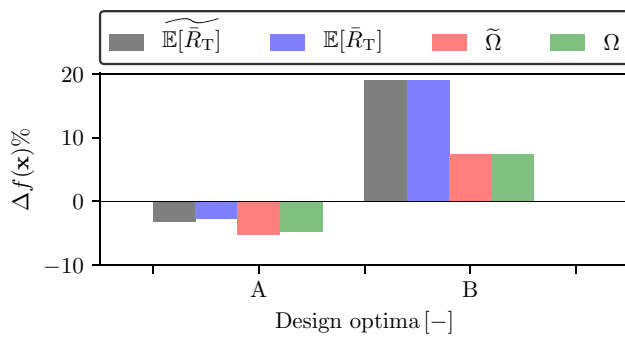


Fig. 21 DDO non-dominated solutions set (top) and optimum designs (bottom)

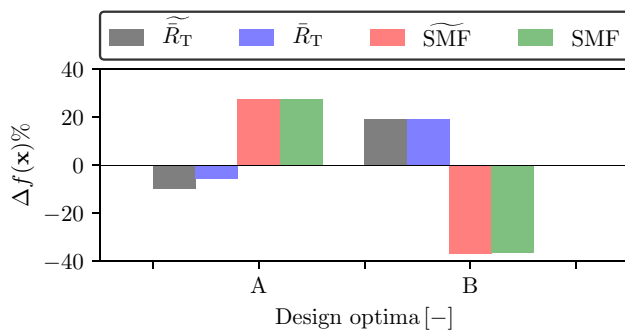


Fig. 22 DDO optima verification: $\widetilde{\cdot}$ represents the metamodel prediction

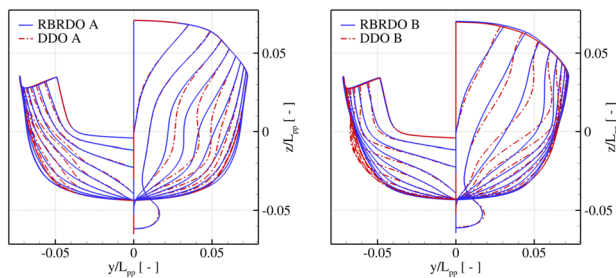


Fig. 23 Comparison of stochastic and deterministic optimal designs

designs A and B are very close or coincident with design-space bounds/corners, meaning that higher improvements could be likely found increasing the design-space bounds and/or adding design variables. In this last case, the cost of the optimization procedure would obviously increase. For the current optimization the computational costs are summarized in Table 10.

7 Conclusions and future work

The synergetic use of design-space dimensionality reduction, adaptive metamodel, uncertainty quantification methods, global multi-objective optimization algorithm enables the high-fidelity hull-form optimization of a destroyer-type vessel in realistic and stochastic ocean conditions. A multi-objective reliability-based robust design optimization (RBRDO) problem is formulated and solved, along with its deterministic counterpart (DDO). The optimization pertains to the minimization of the mean total resistance expected value and the maximization of the ship operability of the DTMB 5415 in a fully stochastic environment (stochastic speed, sea state, and heading). A three-dimensional design space is used, defined by a physics-informed design-space dimensionality reduction procedure. The optimization is performed using a multi-objective deterministic particle swarm optimization algorithm on a stochastic radial basis function metamodel, trained by about 270 URANS and 7,300 linearized strip-theory potential-flow simulations. Gaussian quadrature and metamodel-based importance sampling are used as uncertainty quantification methods.

Design objectives are found completely conflicting. No compromise solution (capable to improve both the objectives at the same time) is identified. Nevertheless, the SBDO is able to provide quite large non-dominated (Pareto) sets and candidate RBRDO and DDO optima are identified at their extrema and verified by URANS and linear strip theory potential flow, providing significant improvement for both objectives: -2.8% mean total resistance expected value (design A) and + 7.4% operability (design B) for the RBRDO problem; -4.9% mean total resistance (design A)

Table 9 Comparison of RBRDO and DDO optima at deterministic conditions via URANS verification

Design	$\Delta R_{CW}\%$	$\Delta \bar{R}_{RW}\%$	$\Delta \bar{R}_{AW}\%$	$RMS(\hat{\xi}_3)\%$	$RMS(\hat{\xi}_5)\%$	$RMS(v_D)\%$	$RMS(a_B)\%$	$RMS(RM_{bow})\%$
RBRDO A	- 4.7	- 4.9	- 5.9	5.7	0.7	4.2	74.	- 1.5
RBRDO B	34.	31.	15.	- 9.2	- 3.8	- 8.4	11.	2.0
DDO A	4.6	- 5.4	- 58.	8.3	- 11.	- 6.0	- 30.	- 5.0
DDO B	16.	19.	34.	- 9.4	- 8.5	- 10.	- 31.	2.0

$\Delta(\cdot)$ Is the variation of the quantity of interest with respect to the original hull

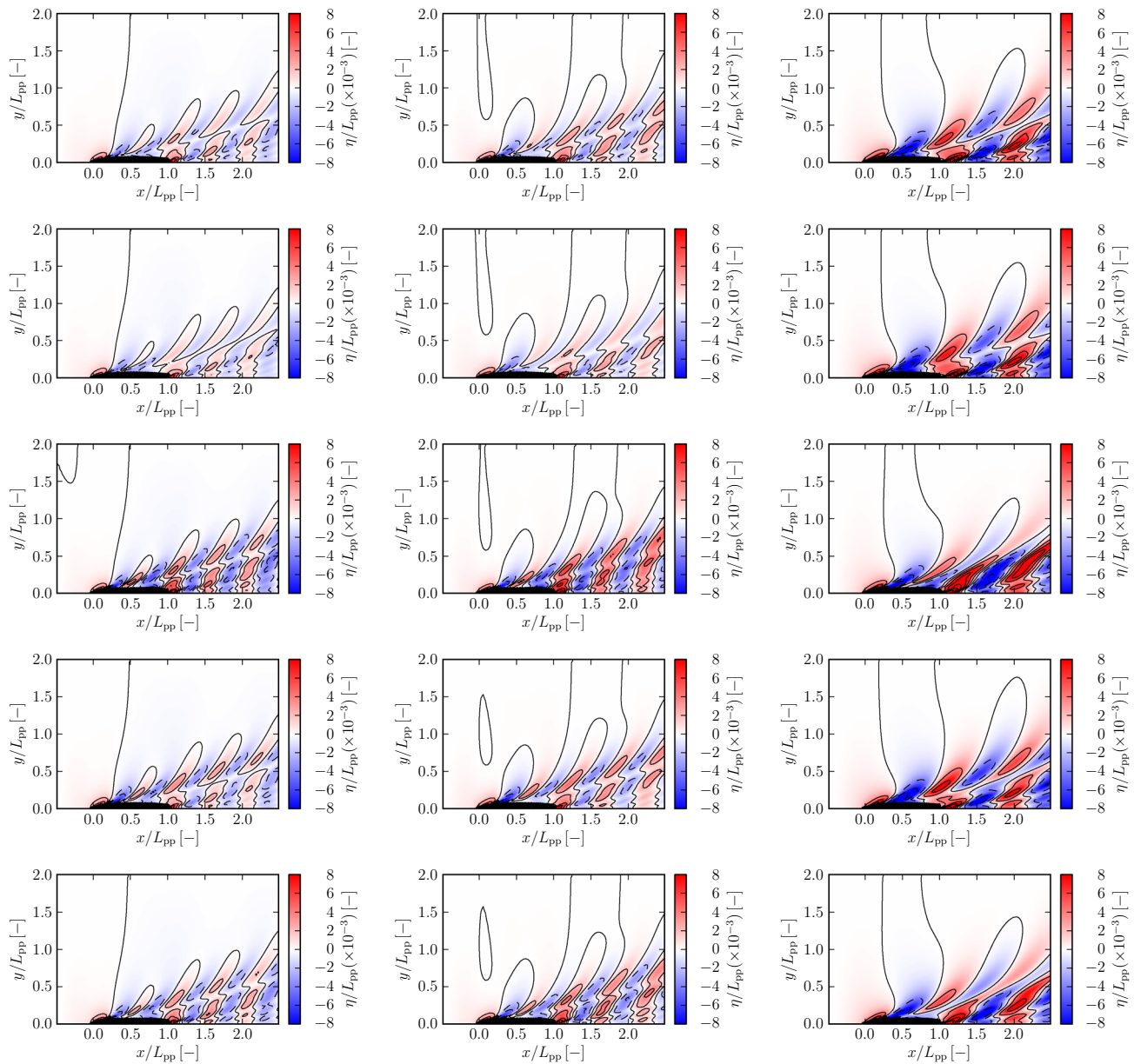


Fig. 24 Calm-water free-surface comparison: (from top to bottom) original, RBRDO (A), RBRDO (B), DDO (A), and DDO (B); (from left to right) $Fr = 0.283$ (stochastic), 0.300 (deterministic), and 0.379 (stochastic)

and -10.5% seakeeping merit factor (design B) for the DDO problem. Compromise solutions and/or higher improvements could be found relaxing the design-space bounds or adding design variables, clearly at the expense of the computational cost.

As discussed, the integration in the SBDO of computational-cost reduction methods has transformed an almost unaffordable problem into a treatable one. Nevertheless, solving this type of high-fidelity stochastic optimization problems likely remains unaffordable for most users in professional and industrial practice, mainly due

to tight constraints in allocating human and technological resources. For this reason, future work will focus on the development and integration of techniques able of further reducing the computational cost of the whole process, such as: non-linear dimensionality reduction methods (e.g., local and kernel PCA, deep autoencoder) [51], multi-fidelity metamodels [56], multi-level/multi-index collocation methods for the forward uncertainty quantification of the simulation outputs [43], and memetic (hybrid global/local) optimization algorithms [42].

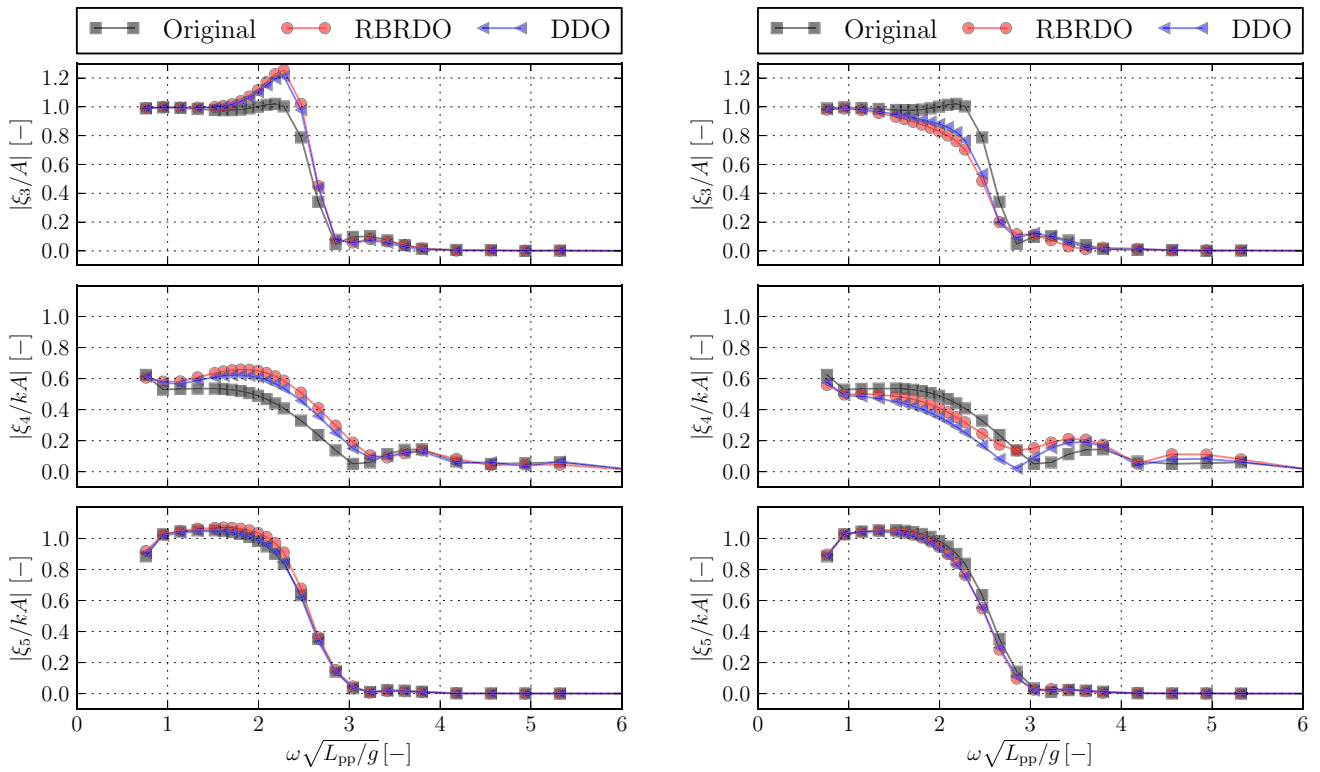


Fig. 25 Original versus RBRDO and DDO optima (left) A and (right) B heave, roll, and pitch transfer functions at deterministic design conditions ($Fr=0.30$; $\beta=0$ for heave and pitch, $\beta=150^\circ$ for roll)

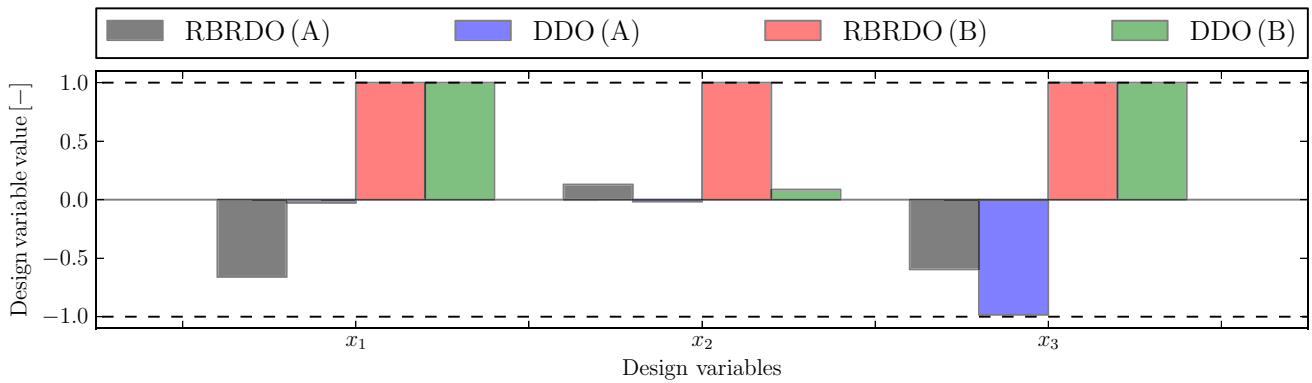


Fig. 26 Optimal design variables for RBRDO and DDO problem

Table 10 Computational cost summary

Computation cost	Original design		Optimization problem	
	Stochastic conditions	Deterministic conditions	RBRDO	DDO
Number of URANS evaluations	10	1	260	78
Number of strip theory evaluations	273	2	7098	52
Total CPU time [h]	46.7 k	3.7 k	363 k	60.5 k

Acknowledgements The work is supported by the US Department of the Navy Office of Naval Research Global, NICOP grant N62909-15-1-2016, administered by Dr. Salahuddin Ahmed, Dr. Elena McCarthy, and Dr. Woei-Min Lin, and by the Italian Flagship Project RITMARE, funded by the Italian Ministry of Education. The research is performed within NATO STO Task Group AVT-252 "Stochastic Design Optimization for Naval and Aero Military Vehicles".

Declarations

Conflict of Interest The authors declare that they have no conflict of interest.

References

- Anderson T, Gerhard K, Sievenpiper B (2013) Operational ship utilization modeling of the DDG-51 class. In: Proceedings of ASNE day 2013 symposia
- Bales SL (1983) Designing ships to the natural environment. *Naval Eng J* 95(2):31–40
- Bassanini P, Bulgarelli U, Campana EF, Lalli F (1994) The wave resistance problem in a boundary integral formulation. *Surv Math Ind* 4:151–194
- Campana EF, Peri D, Tahara Y, Stern F (2006) Shape optimization in ship hydrodynamics using computational fluid dynamics. *Comput Methods Appl Mech Eng* 196(1–3):634–651
- Chen X, Diez M, Kandasamy M, Zhang Z, Campana EF, Stern F (2015) High-fidelity global optimization of shape design by dimensionality reduction, metamodels and deterministic particle swarm. *Eng Optim* 47(4):473–494
- Clerc M (2006) Stagnation analysis in particle swarm optimization or what happens when nothing happens. Technical report. <http://hal.archives-ouvertes.fr/hal-00122031>
- Coello CAC, Pulido GT, Lechuga MS (2004) Handling multiple objectives with particle swarm optimization. *IEEE Trans Evol Comput* 8(3):256–279
- Coppedè A, Gaggero S, Vernengo G, Villa D (2019) Hydrodynamic shape optimization by high fidelity CFD solver and gaussian process based response surface method. *Appl Ocean Res* 90:101841
- Dasgupta D, Michalewicz Z (2013) *Evolutionary algorithms in engineering applications*. Springer, Berlin
- Dawson CW (1977) A practical computer method for solving ship-wave problems. In: Proceedings of the 2nd international conference on numerical ship hydrodynamics, Berkeley, pp 30–38
- Deb K, Jain H (2013) An evolutionary many-objective optimization algorithm using reference-point-based nondominated sorting approach, part i: solving problems with box constraints. *IEEE Trans Evol Comput* 18(4):577–601
- Deb K, Nain PK (2007) An evolutionary multi-objective adaptive meta-modeling procedure using artificial neural networks. *Evolutionary computation in dynamic and uncertain environments*. Springer, Berlin, pp 297–322
- Diez M, Broglia R, Durante D, Olivieri A, Campana EF, Stern F (2018) Statistical assessment and validation of experimental and computational ship response in irregular waves. *J Verif Valid Uncertain Quantif* 3(2):021004
- Diez M, Campana EF, Stern F (2015) Design-space dimensionality reduction in shape optimization by Karhunen-Loève expansion. *Comput Methods Appl Mech Eng* 283:1525–1544
- Diez M, Campana EF, Stern F (2018) Stochastic optimization methods for ship resistance and operational efficiency via CFD. *Struct Multidiscip Optim* 57(2):735–758
- Diez M, He W, Campana EF, Stern F (2014) Uncertainty quantification of delft catamaran resistance, sinkage and trim for variable froude number and geometry using metamodels, quadrature and Karhunen-Loève expansion. *J Mar Sci Technol* 19(2):143–169
- Diez M, Serani A, Stern F, Campana EF (2016) Combined geometry and physics based method for design-space dimensionality reduction in hydrodynamic shape optimization. In: Proceedings of the 31st symposium on naval hydrodynamics, Monterey, CA, USA
- Durante D, Broglia R, Diez M, Olivieri A, Campana E, Stern F (2020) Accurate experimental benchmark study of a catamaran in regular and irregular head waves including uncertainty quantification. *Ocean Eng* 195:106685
- D'Agostino D, Serani A, Diez M (2020) Design-space assessment and dimensionality reduction: an off-line method for shape reparameterization in simulation-based optimization. *Ocean Eng* 197:106852
- Giannakoglou K (2002) Design of optimal aerodynamic shapes using stochastic optimization methods and computational intelligence. *Prog Aerosp Sci* 38(1):43–76
- Grigoropoulos G, Campana E, Diez M, Serani A, Goren O, Sariöz K, Danişman D, Visonneau M, Queutey P, Abdel-Maksoud M, et al. (2017) Mission-based hull-form and propeller optimization of a transom stern destroyer for best performance in the sea environment. In: VII International conference on computational methods in marine engineering MARINE2017
- Harries S, Abt C (2019) Faster turn-around times for the design and optimization of functional surfaces. *Ocean Eng* 193:106470
- He W, Diez M, Zou Z, Campana EF, Stern F (2013) URANS study of delft catamaran total/added resistance, motions and slamming loads in head sea including irregular wave and uncertainty quantification for variable regular wave and geometry. *Ocean Eng* 74:189–217
- Huang J, Carrica PM, Stern F (2008) Semi-coupled air/water immersed boundary approach for curvilinear dynamic overset grids with application to ship hydrodynamics. *Int J Numer Methods Fluids* 58(6):591–624
- Iuliano E, Pérez EA (2016) *Application of surrogate-based global optimization to aerodynamic design*. Springer, Berlin
- Jin R, Chen W, Sudjianto A (2002) On sequential sampling for global metamodeling in engineering design. In: International design engineering technical conferences and computers and information in engineering conference 36223, pp 539–548
- Kennedy J, Eberhart RC (1995) Particle swarm optimization. In: Proceedings of the fourth IEEE conference on neural networks, Piscataway, NJ, pp 1942–1948.
- Kennell CG, White BL, Comstock EN (1985) Innovative naval designs for north atlantic operations. *SNAME Trans* 93:261–281
- Larson J, Menickelly M, Wild SM (2019) Derivative-free optimization methods. *Acta Numer* 28:287–404
- Larsson L, Stern F, Visonneau M, Hirata N, Hino T, Kim J (2015) Proceedings, Tokyo 2015 workshop on cfd in ship hydrodynamics. In: Tokyo CFD workshop
- Lin Y, He J, Li K (2018) Hull form design optimization of twin-skeg fishing vessel for minimum resistance based on surrogate model. *Adv Eng Softw* 123:38–50
- Longo J, Stern F (2005) Uncertainty assessment for towing tank tests with example for surface combatant DTMB model 5415. *J Ship Res* 49(1):55–68
- Lukaczyk T, Palacios F, Alonso JJ, Constantine P (2014) Active subspaces for shape optimization. In: Proceedings of the 10th AIAA multidisciplinary design optimization specialist conference, National Harbor, Maryland, USA, 13–17 January
- Meyers WG, Baitis AE (1985) SMP84: improvements to capability and prediction accuracy of the standard ship motion program

- SMP81. In: Technical report. SPD-0936-04, David Taylor naval ship research and development center
35. Miao A, Zhao M, Wan D (2020) CFD-based multi-objective optimisation of S60 catamaran considering demihull shape and separation. *Appl Ocean Res* 97:102071
 36. Michel WH (1999) Sea spectra revisited. *Mar Technol* 36(4):211–227
 37. Mirjalili S (2016) Dragonfly algorithm: a new meta-heuristic optimization technique for solving single-objective, discrete, and multi-objective problems. *Neural Comput Appl* 27(4):1053–1073
 38. Mirjalili S, Gandomi AH, Mirjalili SZ, Saremi S, Faris H, Mirjalili SM (2017) Salp swarm algorithm: a bio-inspired optimizer for engineering design problems. *Adv Eng Softw* 114:163–191
 39. Mousaviraad SM (2010) CFD prediction of ship response to extreme winds and/or waves. Ph.D. thesis, University of Iowa, Iowa City, Iowa, USA. <http://ir.uiowa.edu/etd/559>
 40. Olivieri A, Pistani F, Avanzini A, Stern F, Penna R (2001) Towing tank, sinkage and trim, boundary layer, wake, and free surface flow around a naval combatant INSEAN 2340 model. In: Technical report, DTIC
 41. Pellegrini R, Serani A, Leotardi C, Iemma U, Campana EF, Diez M (2017) Formulation and parameter selection of multi-objective deterministic particle swarm for simulation-based optimization. *Appl Soft Comput* 58:714–731
 42. Pellegrini R, Serani A, Liuzzi G, Rinaldi F, Lucidi S, Diez M (2020) Hybridization of multi-objective deterministic particle swarm with derivative-free local searches. *Mathematics* 8(4):546
 43. Piazzola C, Tamellini L, Pellegrini R, Broglia R, Serani A, Diez M (2020) Uncertainty quantification of ship resistance via multi-index stochastic collocation and radial basis function surrogates: a comparison. In: AIAA AVIATION 2020 FORUM, p 3160
 44. Pinto A, Peri D, Campana EF (2004) Global optimization algorithms in naval hydrodynamics. *Ship Technol Res* 51(3):123–133
 45. Pinto A, Peri D, Campana EF (2007) Multiobjective optimization of a containership using deterministic particle swarm optimization. *J Ship Res* 51(3):217–228
 46. Quagliarella D, Serani A, Diez M, Pisaroni M, Leyland P, Montagliani L, Iemma U, Gaul NJ, Shin J, Wunsch D, et al. (2019) Benchmarking uncertainty quantification methods using the NACA 2412 airfoil with geometrical and operational uncertainties. In: AIAA Aviation 2019 Forum, p 3555
 47. Raghavan B, Breikopf P, Tourbier Y, Villon P (2013) Towards a space reduction approach for efficient structural shape optimization. *Struct Multidiscip Optim* 48:987–1000
 48. Sahinidis NV (2004) Optimization under uncertainty: state-of-the-art and opportunities. *Comput Chem Eng* 28(6–7):971–983
 49. Schlichting H, Gersten K (2000) Boundary-layer theory. Springer, Berlin
 50. Serani A, Campana EF, Diez M, Stern F (2017) Towards augmented design-space exploration via combined geometry and physics based Karhunen-Loève expansion. In: 18th AIAA/ISSMO multidisciplinary analysis and optimization conference (MA&O), AVIATION 2017. Denver, USA, June 5–9
 51. Serani A, D’Agostino D, Campana EF, Diez M (2019) Assessing the interplay of shape and physical parameters by unsupervised nonlinear dimensionality reduction methods. *J Ship Res* 64(4):313–327
 52. Serani A, Diez M (2017) Are random coefficients needed in particle swarm optimization for simulation-based ship design? In: Proceedings of the 7th international conference on computational methods in marine engineering (Marine 2017)
 53. Serani A, Diez M (2018) Shape optimization under stochastic conditions by design-space augmented dimensionality reduction. In: 19th AIAA/ISSMO multidisciplinary analysis and optimization conference (MA&O), AVIATION 2018. Atlanta, USA, June 25–29
 54. Serani A, Diez M, Wackers J, Visonneau M, Stern F (2019) Stochastic shape optimization via design-space augmented dimensionality reduction and RANS computations. In: AIAA Scitech 2019 Forum. San Diego, California, USA, January 7–11
 55. Serani A, Leotardi C, Iemma U, Campana EF, Fasano G, Diez M (2016) Parameter selection in synchronous and asynchronous deterministic particle swarm optimization for ship hydrodynamics problems. *Appl Soft Comput* 49:313–334
 56. Serani A, Pellegrini R, Wackers J, Jeanson CE, Queutey P, Visonneau M, Diez M (2019) Adaptive multi-fidelity sampling for CFD-based optimisation via radial basis function metamodels. *Int J Comput Fluid Dyn* 33(6–7):237–255
 57. Stern F, Volpi S, Gaul NJ, Choi K, Diez M, Broglia R, Durante D, Campana E, Iemma U (2017) Development and assessment of uncertainty quantification methods for ship hydrodynamics. In: 55th AIAA aerospace sciences meeting, p 1654
 58. Tezdogan T, Shenglong Z, Demirel YK, Liu W, Leping X, Yuyang L, Kurt RE, Djatmiko EB, Incecik A (2018) An investigation into fishing boat optimisation using a hybrid algorithm. *Ocean Eng* 167:204–220
 59. Tezzele M, Salmoiraghi F, Mola A, Rozza G (2018) Dimension reduction in heterogeneous parametric spaces with application to naval engineering shape design problems. *Adv Model Simul Eng Sci* 5(1):25
 60. Theodoridis S (2015) Machine learning: a Bayesian and optimization perspective. Academic Press, New York
 61. Uryasev S, Pardalos PM (2013) Stochastic optimization: algorithms and applications, vol 54. Springer, Berlin
 62. Viana FAC, Simpson TW, Balabanov V, Vasilili T (2014) Special section on multidisciplinary design optimization: metamodeling in multidisciplinary design optimization: How far have we really come? *AIAA J* 52(4):670–690
 63. Volpi S, Diez M, Gaul N, Song H, Iemma U, Choi KK, Campana EF, Stern F (2015) Development and validation of a dynamic metamodel based on stochastic radial basis functions and uncertainty quantification. *Struct Multidiscip Optim* 51(2):347–368
 64. Xing T, Stern F (2010) Factors of safety for Richardson extrapolation. *J Fluids Eng* 132(6):061403
 65. Yang C, Huang F (2016) An overview of simulation-based hydrodynamic design of ship hull forms. *J Hydrodyn Ser B* 28(6):947–960
 66. Yang XS (2011) Metaheuristic optimization: algorithm analysis and open problems. In: International symposium on experimental algorithms, Springer, pp 21–32
 67. Zhang S, Tezdogan T, Zhang B, Xu L, Lai Y (2018) Hull form optimisation in waves based on CFD technique. *Ships Offshore Struct* 13(2):149–164
 68. Zhang S, Zhang B, Tezdogan T, Xu L, Lai Y (2018) Computational fluid dynamics-based hull form optimization using approximation method. *Eng Appl Comput Fluid Mech* 12(1):74–88
 69. Zhao L, Choi K, Lee I (2011) Metamodeling method using dynamic kriging for design optimization. *AIAA J* 49(9):2034–2046

Publisher’s Note Springer Nature remains neutral with regard to jurisdictional claims in published maps and institutional affiliations.